

Longitudinal and transverse mobilities of n -type monolayer transition metal dichalcogenides in the presence of proximity-induced interactions at low temperature

J. Liu,¹ W. Xu,^{1,2,3,*} Y. M. Xiao,^{1,†} L. Ding,¹ H. W. Li,² B. Van Duppen,⁴ M. V. Milošević,⁴ and F. M. Peeters^{2,4}

¹*School of Physics and Astronomy and Yunnan Key laboratory of Quantum Information, Yunnan University, Kunming 650091, China*

²*Micro Optical Instruments Inc., Shenzhen 518118, China*

³*Key Laboratory of Materials Physics, Institute of Solid State Physics, HFIPS, Chinese Academy of Sciences, HFIPS, Hefei 230031, China*

⁴*Department of Physics, University of Antwerp, Groenenborgerlaan 171, B-2020 Antwerpen, Belgium*

(Dated: November 5, 2024)

We present a detailed theoretical investigation on the electronic transport properties of n -type monolayer (ML) transition metal dichalcogenides (TMDs) at low temperature in the presence of proximity-induced interactions such as Rashba spin-orbit coupling (RSOC) and the exchange interaction. The electronic band structure is calculated by solving the Schrödinger equation with a $\mathbf{k} \cdot \mathbf{p}$ Hamiltonian, and the electric screening induced by electron-electron interaction is evaluated under a standard random phase approximation approach. In particular, the longitudinal and transverse or Hall mobilities are calculated by using a momentum-balance equation derived from a semi-classical Boltzmann equation, where the electron-impurity interaction is considered as the principal scattering center at low temperature. The obtained results show that the RSOC can induce the in-plane spin components for spin-split subbands in different valleys, while the exchange interaction can lift the energy degeneracy for electrons in different valleys. The opposite signs of Berry curvatures in the two valleys would introduce opposite directions of Lorentz force on valley electrons. As a result, the transverse currents from nondegenerate valleys can no longer be canceled out so that the transverse current or Hall mobility can be observed. Interestingly, we find that at a fixed effective Zeeman field, the lowest spin-split conduction subband in ML-TMDs can be tuned from one in the K' -valley to one in the K -valley by varying the Rashba parameter. The occupation of electrons in different valleys also varies with changing carrier density. Therefore, we can change the magnitude and direction of the Hall current by varying the Rashba parameter, effective Zeeman field, and carrier density by, e.g., the presence of a ferromagnetic substrate and/or applying a gate voltage. By taking the ML-MoS₂ as an example, these effects are demonstrated and examined. The important and interesting theoretical findings can be beneficial to experimental observation of the valleytronic effect and to gaining an in-depth understanding of the ML-TMDs systems in the presence of proximity-induced interactions.

I. INTRODUCTION

In recent years, the investigation of transition-metal dichalcogenides (TMDs) -based atomically thin two-dimensional (2D) electronic systems has attracted a great deal of attention in condensed-matter physics and nano-electronics communities due to their spintronic and valleytronic properties [1, 2]. These unique and interesting electronic properties are promising for advanced electronics and optoelectronics, with potential applications in next-generation information technology [3–5]. The discovery of 2D TMDs -based valleytronic systems has also led to the proposal and observation of novel physics effects such as the valley Hall effect (VHE) [1, 6, 7], which is electrically equivalent to the Hall effect observed in the presence of an external perpendicular magnetic field. One of the most interesting features of a free-standing valleytronic material is that the electron energies are degenerated around K and K' points in the electronic band

structure [8–10]. However, the electronic spin orientations around these two valleys are just the opposite [11]. Thus, the electronic band structure exhibits Berry curvature [1, 12], and the electrons with different spin orientations can move along different directions under the action of a driving electric field and/or a polarized electromagnetic (EM) field [13, 14]. Hence, the experimental techniques for the measurement of the VHE are similar to those used for the detection of the spin Hall effect in spintronic systems in the absence of an external magnetic field [15].

The VHE has been observed experimentally in 2D TMDs systems normally in the presence of driving EM field. This enables the electrical and optical detections and manipulation of the photo-induced valley current in valleytronic systems [16]. However, at present the experimental observation of the VHE by directly using the electric transport measurement has been unsuccessful. There is also the lack of related theoretical investigation to address this problem. From a viewpoint of condensed matter physics, in an inversion symmetric breaking 2D ML-TMDs system with energy degeneracy around K - and K' -point, under the action of a driving electric field the current densities induced by electron movement from two

* wenxu_issp@aliyun.com

† yiming.xiao@ynu.edu.cn

valleys are equal in magnitude but with opposite directions due to different signs of Berry curvatures. As a result, the overall transverse or Hall voltage is canceled out and the VHE cannot be observed by conventional transport measurement. A way out of this situation is by breaking or lifting the valley degeneracy. One of the most efficient schemes to lift the valley degeneracy in a 2D TMDs material is to place the ML-TMDs film on a dielectric or ferromagnetic substrate [17, 18]. In such a case, the proximity effect induced by the presence of the substrate can result in not only the Rashba spin-orbit coupling (RSOC) [19–21] but also the exchange interaction with an effective Zeeman field (EZF) [22]. The RSOC can induce the in-plane electronic spin and the corresponding modification of spin splitting in the electronic band structure in a ML-TMDs. This can be utilized for the access and manipulation of valleys and spins in a 2D ML-TMDs/substrate system. Furthermore, the proximity induced exchange interaction can lift the valley degeneracy in the electronic energy spectra due to the introduction of a magnetic momentum and/or van der Waals force in a 2D ML-TMDs system. When the energy degeneracy in different valleys is lifted, the valley currents from different valleys with different orientations can no longer be canceled out. Thus, the electric voltage can be measured in transverse direction and, hence, the VHE can be observed under the action of a dc electric field. Consequently, in the presence of a particular substrate the proximity induced interactions can be utilized for directly observation of the VHE in 2D ML-TMDs systems using conventional transport measurement, namely applying an electric current/voltage along the x -direction and measuring the voltage/current along the y -direction. When the resistance R_{xy} or conductance σ_{xy} is nonzero, the electric VHE is observed.

Very recently, we have constructed an electron Hamiltonian in which the RSOC and the EZF induced by proximity effects are considered for ML-TMDs under the standard $\mathbf{k} \cdot \mathbf{p}$ approximation [23]. It has been demonstrated that in the presence of RSOC and EZF, the electronic band structure in ML-TMDs depends strongly on the proximity-induced interactions and the optical Hall effect can be observed by applying the linearly polarized EM radiation field on a ML-TMDs [23], where a non-zero optical conductivity $\sigma_{xy}(\omega)$ can be measured and the sign of the optical Hall current or polarization can be tuned by varying the Rashba parameter. In this study, we evaluate the longitudinal and transverse mobilities in a ML-TMDs system by including the proximity-induced RSOC and exchange interaction. We take the ML-MoS₂ as an example to examine the dependence of the electronic screening and the longitudinal and transverse mobilities upon the strengthes of the RSOC and the EZF. The prime motivation of this study is to see under what conditions the VHE can be observed by direct electric transport measurement and whether this effect is experimentally measurable. The paper is organized as follows. The theoretical approaches developed in this study are

presented in Sec. II, where we derive the formulas for the calculations of the electronic band structure, Berry curvature, the inverse electronic screening length, and the longitudinal and transverse or Hall mobilities. The obtained results are presented and discussed in Sec. III and the concluding remarks are summarized in Sec. IV.

II. THEORETICAL APPROACH

A. Electronic band structure and Berry curvature

In this study, we consider a ML-TMDs placed on a substrate with which the proximity-induced interactions can lead to the enhancements of the valley splitting and to Rashba spin-orbit coupling (SOC). We take an effective low- electron energy Hamiltonian that includes the effect of RSOC and EZF induced by the proximity interactions. The Hamiltonian for an electron in a ML-TMDs/substrate heterostructure system consists of four parts[21, 23, 24]:

$$H = H_0 + H_{\text{SOC}} + H_{\text{ex}} + H_R, \quad (1)$$

where H_0 originates from the electronic orbital interaction, H_{SOC} is the intrinsic SOC in the system, H_{ex} is attributable to the exchange interaction, and H_R is the contribution from the RSOC. As we know, ML-TMDs is a 2D hexagonal crystal with uniaxial symmetry where the RSOC always exists [25, 26]. When the ML-TMDs is placed on a substrate, the presence of the heterostructure can lead to the breaking of the inversion symmetry along the direction normal to the 2D plane of the ML-TMDs [21, 22]. This can further enhance the RSOC [27–29]. Furthermore, the presence of the dielectric and/or ferromagnetic substrate can result in an exchange interaction between the ML-TMDs and the substrate. The exchange interaction is due to the introduction of EZF by the van der Waals force in the film/substrate heterostructure [22] and adds the H_{ex} term into Eq. (1). Meanwhile, the above Hamiltonian can be written in the form of a 4×4 matrix given as [23]

$$H^\zeta(\mathbf{k}) = \frac{1}{2} \times \begin{bmatrix} \Delta + d_\zeta^c & 2Ak_\zeta^- & 0 & i(1 - \zeta)\lambda_R \\ 2Ak_\zeta^+ & d_\zeta^v - \Delta & -i(1 + \zeta)\lambda_R & 0 \\ 0 & i(1 + \zeta)\lambda_R & \Delta - d_\zeta^c & 2Ak_\zeta^- \\ i(\zeta - 1)\lambda_R & 0 & 2Ak_\zeta^+ & -(\Delta + d_\zeta^v) \end{bmatrix}, \quad (2)$$

where $\zeta = \pm$ refers to the K (K') valley, $\mathbf{k} = (k_x, k_y)$ is the electron wave vector along the 2D-plane, $k_\zeta^\pm = \zeta k_x \pm ik_y$, Δ is the direct band gap between the conduction and valence bands, and $A = at$, with a being the lattice parameter and t the hopping parameter [1, 30, 31]. Furthermore, $d_\zeta^\beta = \zeta\lambda_\beta - B_\beta$, where $\beta = (c, v)$ refers to the conduction and valence band, respectively. The

intrinsic SOC parameter $2\lambda_c$ is the spin splitting at the bottom of the conduction band, and $2\lambda_v$ is that at the top of the valence band in the absence of the RSOC [1, 32]. B_c and B_v are the EZF experienced by an electron in the conduction and valence bands in the presence of exchange interaction. $\lambda_R = \alpha_R \Delta / (2at)$ comes from the RSOC, with α_R being the Rashba parameter [33, 34]. The corresponding Schrödinger equation for a carrier in a ML-TMDs system near the K (K') valley can be solved analytically. The four eigenvalues, $E = E_{\beta,s}^c(\mathbf{k})$, with $s = \pm$ being the spin index, are the solutions of the diagonalized equation of the matrix, which reads

$$E^4 - A_2 E^2 + A_1 E + A_0 = 0, \quad (3)$$

with

$$\begin{aligned} A_2 &= \Delta^2/2 + \lambda_R^2 + 2A^2 k^2 + (d_\zeta^v{}^2 + d_\zeta^c{}^2)/4, \\ A_1 &= \Delta(d_\zeta^v{}^2 - d_\zeta^c{}^2)/4 - \zeta \lambda_R^2 (d_\zeta^v - d_\zeta^c)/2, \\ A_0 &= (\Delta^2/4 + A^2 k^2)^2 + \lambda_R^2 (\Delta + \zeta d_\zeta^c) (\Delta + \zeta d_\zeta^d)/4 \\ &\quad - \Delta^2 (d_\zeta^c{}^2 + d_\zeta^v{}^2)/16 - A^2 k^2 d_\zeta^c d_\zeta^v/2 + (d_\zeta^c d_\zeta^v)^2/16. \end{aligned}$$

The corresponding eigenfunctions for an electronic state near the K and K' points are

$$|\mathbf{k}; \lambda \rangle = \mathcal{A}_{\beta,s}^c [c_1, c_2, c_3, c_4] e^{i\mathbf{k} \cdot \mathbf{r}}, \quad (4)$$

where $\mathbf{r} = (x, y)$, $\lambda = (\beta, \zeta, s)$,

$$\begin{aligned} c_1 &= i\lambda_R [h_1 + 4A^2(1 + \zeta)(k_\zeta^-)^2], \\ c_2 &= -4iA\lambda_R k_\zeta^- h_2, \\ c_3 &= 2Ak_\zeta^- h_3, \\ c_4 &= -[(\Delta - 2E)^2 - (d_\zeta^c)^2](\Delta + 2E - d_\zeta^c) \\ &\quad - (1 + \zeta)^2 \lambda_R^2 (\Delta - 2E + d_\zeta^c) \\ &\quad - 4A^2 k^2 (\Delta - 2E - d_\zeta^c), \end{aligned}$$

and $\mathcal{A}_{\beta,s}^c(\mathbf{k}) = (|c_1|^2 + |c_2|^2 + |c_3|^2 + |c_4|^2)^{-1/2}$ is the normalization coefficient. Here, $h_1 = (1 - \zeta)(\Delta - 2E - d_\zeta^c)(\Delta + 2E - d_\zeta^c)$, $h_2 = \Delta - 2E + \zeta d_\zeta^c$, and $h_3 = (\Delta - 2E + d_\zeta^c)(\Delta + 2E - d_\zeta^v) + 4A^2 k^2$. As we know, the Rashba term H_R can lead to the projection of the spin component in the x - y plane and mixes the spin states. Therefore, the spin index s is no longer a good quantum number [21, 35], and thus we use $s = \pm$ for up/down for the sake of distinguishing different electronic states induced by RSOC.

As we known, the Berry curvature can significantly modify the electron dynamics and generate new electrical transport phenomena by introducing an effective magnetic field. For a free-standing ML-TMDs, the electrons in the two valleys experience effective magnetic fields proportional to the Berry curvatures with equal magnitudes but opposite signs due to the broken inversion symmetry in its crystal structure [1, 13, 16]. However, the presence of proximity-induced interactions such as RSOC and

exchange interaction would also modify the Berry curvature behaviors. With eigenvalues and eigenfunctions obtained from Eqs.(3) and (4), the Berry curvature of ML-TMDs in the presence of the proximity-induced interactions $\mathbf{\Omega}_\lambda(\mathbf{k}) = \nabla_{\mathbf{k}} \times i \langle \mathbf{k}; \lambda | \nabla_{\mathbf{k}} | \mathbf{k}; \lambda \rangle \cdot \hat{\mathbf{z}}$ at each valley can be calculated through [36]

$$\begin{aligned} \mathbf{\Omega}_{\beta,s}^\zeta(\mathbf{k}) &= i \sum_{\beta',s'}' \left[\frac{\langle \mathbf{k}; \lambda | \partial H / \partial k_x | \mathbf{k}; \lambda' \rangle \langle \mathbf{k}; \lambda' | \partial H / \partial k_y | \mathbf{k}; \lambda \rangle}{[E_{\beta,s}^\zeta(\mathbf{k}) - E_{\beta',s'}^\zeta(\mathbf{k})]^2} \right. \\ &\quad \left. - \left(\frac{\partial}{\partial k_x} \leftrightarrow \frac{\partial}{\partial k_y} \right) \right], \end{aligned} \quad (5)$$

where the prime symbol ($'$) above \sum is introduced to denote the exclusion of the case $(\beta', s') = (\beta, s)$.

B. Electron-electron interaction and electronic screening

With the electron wave-function and the energy spectrum, we can evaluate the electrostatic energy induced by electron-electron (e-e) interaction and the dynamical dielectric function under the usual random-phase approximation (RPA). From now on, we consider an n -type ML-TMDs system in which the conducting carriers are electrons in the conduction band. Taking only the spin splitting conduction band (i.e., $\beta = c$ only) into account, we use the notations $\psi_{\mathbf{s}\mathbf{k}}^\zeta(\mathbf{r})$ and $E_s^\zeta(\mathbf{k})$ for the electron wave function and the energy spectrum, respectively, at a state $|\mathbf{k}; \zeta, s\rangle$ in the conduction band. As a result, we are now dealing with a two-band situation around the K or K' points. The electrostatic potential induced by the bare e-e interaction via the Coulomb interaction $V(\mathbf{r}) = e^2/(\kappa|\mathbf{r}|)$ can be calculated via

$$\begin{aligned} V_{s's}^\zeta(\mathbf{k}, \mathbf{q}) &= \langle \psi_{s'\mathbf{k}_1+\mathbf{q}}^{\zeta*}(\mathbf{r}_1) \psi_{s\mathbf{k}_1}^\zeta(\mathbf{r}_1) | V(\mathbf{r}_1 - \mathbf{r}_2) \\ &\quad | \psi_{s\mathbf{k}_2}^{\zeta*}(\mathbf{r}_2) \psi_{s'\mathbf{k}_2+\mathbf{q}}^\zeta(\mathbf{r}_2) \rangle = V_q F_{s's}^\zeta(\mathbf{k}, \mathbf{q}). \end{aligned} \quad (6)$$

Here, the conservation law for momentum flowing into and out of the interaction has been applied, κ is the dielectric constant for a ML-TMDs material, $\mathbf{q} = (q_x, q_y)$ is the change of the electron wavevector during an e-e scattering event, $V_q = 2\pi e^2/(\kappa q)$ is the 2D Fourier transformation of the Coulomb potential induced by e-e interaction, and

$$\begin{aligned} F_{ss'}^\zeta(\mathbf{k}, \mathbf{q}) &= [\mathcal{A}_{s'}^\zeta(\mathbf{k} + \mathbf{q}) \mathcal{A}_s^\zeta(\mathbf{k})]^2 \sum_{i=1}^4 c_{is}^{\zeta*}(\mathbf{k}) c_{is'}^\zeta(\mathbf{k} + \mathbf{q}) \\ &\quad \times \sum_{j=1}^4 c_{js'}^{\zeta*}(\mathbf{k} + \mathbf{q}) c_{js}^\zeta(\mathbf{k}), \end{aligned} \quad (7)$$

is the form factor for many-body interaction, where $\mathcal{A}_s^\zeta(\mathbf{k}) = \mathcal{A}_{c,s}^\zeta(\mathbf{k})$ and the hybridization of the four electron wave functions, given by Eq. (4), at a state $|\mathbf{k}; \zeta, s\rangle$ has been included.

With the electrostatic potential induced by bare e-e interaction, the dynamical dielectric function for electrons in spin split conduction band in valley ζ can be calculated by the RPA approach, which is given by a 2×2 matrix as

$$\varepsilon_\zeta(\Omega, \mathbf{q}) = \begin{bmatrix} 1 - A_{--} & A_{-+} \\ A_{+-} & 1 - A_{++} \end{bmatrix}, \quad (8)$$

where $A_{ss'} = A_{ss'}^\zeta(\Omega, \mathbf{q}) = V_q \sum_{\mathbf{k}} F_{ss'}^\zeta(\mathbf{k}, \mathbf{q}) \Pi_{ss'}^\zeta(\Omega; \mathbf{k}, \mathbf{q})$ is for scattering of an electron in a split state s to a split state s' , Ω is the excitation frequency, and

$$\Pi_{s's}^\zeta(\Omega; \mathbf{k}, \mathbf{q}) = \frac{f[E_{s'}^\zeta(\mathbf{k} + \mathbf{q})] - f[E_s^\zeta(\mathbf{k})]}{E_{s'}^\zeta(\mathbf{k} + \mathbf{q}) - E_s^\zeta(\mathbf{k}) + \hbar\Omega + i\delta}, \quad (9)$$

is the corresponding density-density (d-d) correlation function (or pair bubble) with $f(x) = [e^{(x-E_F)/k_B T} + 1]^{-1}$ being the Fermi-Dirac function and E_F the Fermi energy or chemical potential.

In a static case ($\Omega \rightarrow 0$) and long-wavelength limit ($q \rightarrow 0$), the real part of the d-d correlation function becomes

$$D_{ss}^\zeta(\mathbf{k}) = \lim_{q \rightarrow 0} \text{Re} \Pi_{ss}^\zeta(0; \mathbf{k}, \mathbf{q}) \simeq \left. \frac{\partial f(x)}{\partial x} \right|_{x=E_s^\zeta(\mathbf{k})}, \quad (10)$$

for intra-subband ($s' = s$) transition, and

$$D_{s's}^\zeta(\mathbf{k}) = \lim_{q \rightarrow 0} \text{Re} \Pi_{s's}^\zeta(0; \mathbf{k}, \mathbf{q}) \simeq \frac{f[E_{s'}^\zeta(\mathbf{k})] - f[E_s^\zeta(\mathbf{k})]}{E_{s'}^\zeta(\mathbf{k}) - E_s^\zeta(\mathbf{k})}, \quad (11)$$

for inter-subband ($s \neq s'$) transition, respectively.

By definition, the effective e-e interaction potential in the presence of electronic screening can be calculated through a matrix:

$$[\mathcal{V}_{ss'}^\zeta(\mathbf{k}, \mathbf{q})] = [V_{ss'}^\zeta(\mathbf{k}, \mathbf{q})][\text{Re} \varepsilon_\zeta(0, \mathbf{q})]^{-1}, \quad (12)$$

which reads

$$\begin{aligned} [\mathcal{V}_{ss'}^\zeta(\mathbf{k}, \mathbf{q})] &= \begin{bmatrix} \mathcal{V}_{--} & \mathcal{V}_{-+} \\ \mathcal{V}_{+-} & \mathcal{V}_{++} \end{bmatrix} = \begin{bmatrix} V_{--} & V_{-+} \\ V_{+-} & V_{++} \end{bmatrix} \begin{bmatrix} 1 - A_{--}^{(1)} & A_{-+}^{(1)} \\ A_{+-}^{(1)} & 1 - A_{++}^{(1)} \end{bmatrix}^{-1} \\ &= \frac{2\pi e^2}{\kappa \mathcal{Q}^2} \begin{bmatrix} F_{--}^\zeta(q + K_{++}^\zeta) + F_{-+}^\zeta(K_{+-}^\zeta) & F_{-+}^\zeta(q + K_{--}^\zeta) + F_{--}^\zeta(K_{+-}^\zeta) \\ F_{+-}^\zeta(q + K_{++}^\zeta) + F_{++}^\zeta(K_{+-}^\zeta) & F_{++}^\zeta(q + K_{--}^\zeta) + F_{+-}^\zeta(K_{+-}^\zeta) \end{bmatrix}, \end{aligned} \quad (13)$$

where $A_{ss'}^{(1)} = \text{Re} A_{ss'} = V_q \sum_{\mathbf{k}} F_{ss'}^\zeta(\mathbf{k}, \mathbf{q}) \text{Re} \Pi_{ss'}^\zeta(0; \mathbf{k}, \mathbf{q})$ and $\mathcal{Q}^2 = (q + K_{--})(q + K_{++}) - K_{-+}K_{+-}$. The inverse static screening length is defined as

$$\begin{aligned} K_{ss'}^\zeta &= K_{ss'}^\zeta(\mathbf{q}) = -qV_q \sum_{\mathbf{k}} F_{ss'}^\zeta(\mathbf{k}, \mathbf{q}) \text{Re} \Pi_{ss'}^\zeta(0, \mathbf{k}, \mathbf{q}) \\ &= -\frac{2\pi e^2}{\kappa} \sum_{\mathbf{k}} F_{ss'}^\zeta(\mathbf{k}, \mathbf{q}) \text{Re} \Pi_{ss'}^\zeta(0, \mathbf{k}, \mathbf{q}), \end{aligned} \quad (14)$$

which implies that different electronic transition channels correspond to different screening lengths. Eq. (14) reflects a fact that in the presence of electronic screening the effective electronic transition from s to s' spin states should, in principle, be affected by other transition events. In the long-wavelength limit ($q \rightarrow 0$) we have $F_{ss}^\zeta(\mathbf{k}, \mathbf{q}) \rightarrow 1$ for $s = s'$ because of the normalization of the wave function, and $F_{s's}^\zeta(\mathbf{k}, \mathbf{q}) \rightarrow 0$ and $K_{s's}^\zeta(\mathbf{q}) \rightarrow 0$ for $s \neq s'$ because of the orthogonality of the electron wave function. In such a case, Eq. (13) becomes

$$\begin{bmatrix} \mathcal{V}_{--} & \mathcal{V}_{-+} \\ \mathcal{V}_{+-} & \mathcal{V}_{++} \end{bmatrix} = \frac{2\pi e^2}{\kappa} \begin{bmatrix} (q + K_{--}^\zeta)^{-1} & 0 \\ 0 & (q + K_{++}^\zeta)^{-1} \end{bmatrix}, \quad (15)$$

where

$$K_{ss}^\zeta = -(2\pi e^2/\kappa) \sum_{\mathbf{k}} [\partial f(x)/\partial x]_{x=E_s^\zeta(\mathbf{k})}, \quad (16)$$

is the inverse screening length which is independent of \mathbf{k} and \mathbf{q} . This result indicates that in the long-wavelength limit the effective e-e interaction and the electronic screening can only be caused via intra-subband electronic transitions. The inter-subband transitions, corresponding to spin-flip transitions, can only be achieved with the change of electron momentum during the scattering events.

C. Electronic transport coefficients

In this study, we employ a simple Boltzmann equation (BE) approach to calculate the transport coefficient for a ML-TMDs in the presence of proximity induced interactions. In the present study, we neglect the electronic transitions between different valleys, because these transition channels require a big change of electron momentum that is less possible in the transport experiment under the action of a relatively weak driving dc electric field. For an n -type ML-TMDs with a spin splitting conduction band, a two-band model is required to describe the electronic properties in splitting bands. The time-independent semi-classical Boltzmann equation can be

written as

$$-\frac{e}{\hbar}\mathbf{F}\cdot\nabla_{\mathbf{k}}f_s^\zeta(\mathbf{k})=\sum_{\mathbf{k}',s'}[\mathbf{F}_{s',s}^\zeta(\mathbf{k}',\mathbf{k})-\mathbf{F}_{s',s}^\zeta(\mathbf{k},\mathbf{k}')], \quad (17)$$

where \mathbf{F} is a force acting on the electron, $f_s^\zeta(\mathbf{k})$ is the momentum distribution function (MDF) for an electron in a state $|\mathbf{k};\zeta,s\rangle$, $F_{s',s}^\zeta(\mathbf{k},\mathbf{k}')=f_s^\zeta(\mathbf{k})W_{s',s}^\zeta(\mathbf{k},\mathbf{k}')$, and $W_{s',s}^\zeta(\mathbf{k},\mathbf{k}')$ is the electronic transition rate for scattering of an electron from a state $|\mathbf{k};\zeta,s\rangle$ to a state $|\mathbf{k}';\zeta,s'\rangle$ in the conduction band due to the presence of electronic scattering centers such as impurities and phonons. When an electric field is applied along the x -direction of the ML-TMDs, $\mathbf{F}=F(1,0,0)$ is the strength of the dc electric field and we obtain

$$\mathbf{F}\cdot\nabla_{\mathbf{k}}f_s^\zeta(\mathbf{k})=F\frac{\partial f_s^\zeta(\mathbf{k})}{\partial k_x}. \quad (18)$$

For the first moment, the momentum-balance equation can be derived by multiplying $\sum_{s,\mathbf{k}}(k_x,k_y)$ to both sides of the Boltzmann equation given by Eq. (17), which reads

$$\frac{en_e^\zeta}{\hbar}(F,0)=\sum_{s',s,\mathbf{k}',\mathbf{k}}(k'_x-k_x,k'_y-k_y)F_{s',s}^\zeta(\mathbf{k},\mathbf{k}'), \quad (19)$$

where $n_e^\zeta=\sum_{s,\mathbf{k}}f_s^\zeta(\mathbf{k})$ is the electron density in valley ζ . It should be noted that the main effect of driving electric field F is to cause the drift velocities of the electrons in different bands $\mathbf{v}_s^\zeta=(v_{sx}^\zeta,v_{sy}^\zeta)$. As a result, the electron wave vector in the MDF is shifted by $\mathbf{k}\rightarrow\mathbf{k}_s^\zeta=\mathbf{k}-m_s^\zeta\mathbf{v}_s^\zeta/\hbar$, with m_s^ζ being the transport effective mass for an electron in the (s,ζ) band. As we know, the electrons in a solid can be accelerated by a driving electric field. Thus, the electrons in the bottom of the conduction band would move to higher energy states with nonzero k . The electron effective mass under such a condition would usually differ from the band mass in a parabolic low-energy regime. This effective electron mass is often called the transport effective mass. We note here that in general, the transport effective mass for an electron differs from the band effective mass m^* obtained from taking $1/m^*=(1/\hbar^2)d^2E/d^2k$ in an electronic system. $m^*=m_s^\zeta$ normally holds for the case of $E(k)=\hbar^2k^2/(2m^*)$. For the case of a relatively weak driving electric field F , the drift velocity of electron is relatively small so that

$$f_s^\zeta(\mathbf{k}_s^\zeta)\simeq f_s^\zeta(\mathbf{k})-\frac{m_s^\zeta}{\hbar}\left[v_{sx}^\zeta\frac{\partial f_s^\zeta(\mathbf{k})}{\partial k_x}+v_{sy}^\zeta\frac{\partial f_s^\zeta(\mathbf{k})}{\partial k_y}\right]. \quad (20)$$

Thus, we obtain from Eq. (19) that

$$(F,0)=-\sum_{s',s}\frac{m_s^\zeta}{e}(v_{sx}^\zeta S_{ss'}^{\zeta x}+v_{sy}^\zeta T_{ss'}^{\zeta y},v_{sx}^\zeta T_{ss'}^{\zeta x}+v_{sy}^\zeta S_{ss'}^{\zeta y}), \quad (21)$$

where

$$[S_{ss'}^{\zeta\alpha},T_{ss'}^{\zeta\alpha}]=\frac{1}{n_e^\zeta}\sum_{\mathbf{k}',\mathbf{k}}(k'_\alpha-k_\alpha)W_{ss'}^\zeta(\mathbf{k},\mathbf{k}')\times\left[\frac{\partial f_s^\zeta(\mathbf{k})}{\partial k_\alpha},\frac{\partial f_s^\zeta(\mathbf{k})}{\partial k_{\alpha'}}\right], \quad (22)$$

with $\alpha=x$ or y and $\alpha'\neq\alpha$, presents the scattering probability for an electron moving along different directions in different spin and valley subbands. Assuming that the electron MDF can be described by a statistical energy distribution function (EDF) such as the Fermi-Dirac function, we have $f_s^\zeta(\mathbf{k})\simeq f[E_s^\zeta(\mathbf{k})]$ with $f(x)=[e^{(x-E_F)/k_B T}+1]^{-1}$. In an n -type ML-TMDs at the steady state, the single Fermi level is across the system. Thus, we obtain

$$[S_{ss'}^{\zeta\alpha},T_{ss'}^{\zeta\alpha}]=\frac{1}{n_e^\zeta}\sum_{\mathbf{k}',\mathbf{k}}(k'_\alpha-k_\alpha)W_{ss'}^\zeta(\mathbf{k},\mathbf{k}')\times\left[\frac{\partial E_s^\zeta(\mathbf{k})}{\partial k_\alpha},\frac{\partial E_s^\zeta(\mathbf{k})}{\partial k_{\alpha'}}\right]\frac{df(x)}{dx}\Big|_{x=E_s^\zeta(\mathbf{k})}. \quad (23)$$

From Eq. (3), we have

$$\frac{\partial E_s^\zeta(\mathbf{k})}{\partial k_\alpha}=A^2k_\alpha G_s^\zeta(\mathbf{k}), \quad (24)$$

with

$$G_s^\zeta(\mathbf{k})=\frac{4[E_s^\zeta(\mathbf{k})]^2-4A^2k^2-\Delta^2-d_\zeta^c d_\zeta^v}{4[E_s^\zeta(\mathbf{k})]^3-2A_2E_s^\zeta(\mathbf{k})+A_1}, \quad (25)$$

and

$$[S_{ss'}^{\zeta\alpha},T_{ss'}^{\zeta\alpha}]=\frac{A^2}{n_e^\zeta}\sum_{\mathbf{k}',\mathbf{k}}(k'_\alpha-k_\alpha)[k_\alpha,k_{\alpha'}]G_s^\zeta(\mathbf{k})\times W_{ss'}^\zeta(\mathbf{k},\mathbf{k}')\frac{df(x)}{dx}\Big|_{x=E_s^\zeta(\mathbf{k})}. \quad (26)$$

By definition, the current density for electrons in band (s,ζ) is $j_{s\alpha}^\zeta=-e^2n_s^\zeta v_{s\alpha}^\zeta$ along the α direction, with n_s^ζ being the electron density at (ζ,s) state. Using the Onsager relation, Eq. (26) gives

$$\begin{aligned} \begin{bmatrix} \rho_{xx}^\zeta & \rho_{xy}^\zeta \\ \rho_{yx}^\zeta & \rho_{yy}^\zeta \end{bmatrix} &= \sum_s \begin{bmatrix} \rho_{xx}^{s\zeta} & \rho_{xy}^{s\zeta} \\ \rho_{yx}^{s\zeta} & \rho_{yy}^{s\zeta} \end{bmatrix} \\ &= \frac{m_s^\zeta}{e^2 n_s^\zeta} \sum_{s,s'} \begin{bmatrix} S_{ss'}^{\zeta x} & T_{ss'}^{\zeta x} \\ T_{ss'}^{\zeta y} & S_{ss'}^{\zeta y} \end{bmatrix}, \end{aligned} \quad (27)$$

where $\rho_{\alpha\alpha'}^{s\zeta}$ is the longitudinal ($\alpha=\alpha'$) or transverse ($\alpha\neq\alpha'$) resistivity in the band (ζ,s) . Noting that $\rho_{\alpha\alpha'}^{s\zeta}=m_s^\zeta\lambda_{\alpha\alpha'}^{s\zeta}/(e^2n_s^\zeta)$ with $\lambda_{\alpha\alpha'}^{s\zeta}$ being the electronic scattering rate in the band (ζ,s) along different directions, we obtain

$$\begin{bmatrix} \lambda_{xx}^{s\zeta} & \lambda_{xy}^{s\zeta} \\ \lambda_{yx}^{s\zeta} & \lambda_{yy}^{s\zeta} \end{bmatrix} = \sum_{s'} \begin{bmatrix} S_{ss'}^{\zeta x} & T_{ss'}^{\zeta x} \\ T_{ss'}^{\zeta y} & S_{ss'}^{\zeta y} \end{bmatrix}. \quad (28)$$

The electron mobility is defined as $\mu_{\alpha\alpha'}^{\zeta s} = e\tau_{\alpha\alpha'}^{\zeta s}/m_s^{\zeta}$, with $\tau_{\alpha\alpha'}^{\zeta s} = 1/\lambda_{\alpha\alpha'}^{\zeta s}$ being the momentum relaxation time or lifetime for an electron in band (ζ, s) along different directions. Finally, the average longitudinal and transverse or Hall mobilities are given by

$$\mu_{xx} = \frac{n_+^+\mu_{xx}^{++} + n_+^-\mu_{xx}^{-+} + n_-^+\mu_{xx}^{+-} + n_-^-\mu_{xx}^{--}}{n_e}, \quad (29)$$

and

$$\mu_{xy} = \frac{n_+^-\mu_{xy}^{-+} + n_-^-\mu_{xy}^{--} - n_+^+\mu_{xy}^{++} - n_-^+\mu_{xy}^{+-}}{n_e}, \quad (30)$$

respectively, where $n_e = \sum_{\zeta, s} n_s^{\zeta}$ is the total electron density in the system. For average μ_{xy} the electric currents in different directions with different valley indexes are considered. Here we take the standard definition of the elements in the mobility tensor as $\mu_{\alpha\alpha'} = v_{\alpha'}/F_{\alpha}$ with the electron drift velocity (or current) measured along the α' -direction and the driving electric field strength (or applied voltage) along the α -direction.

D. Electron-impurity scattering

At relatively low temperatures, the electron-impurity (e-i) scattering is the principal channel for relaxation of electrons in an electronic system in the presence of a driving electric field. For the case in which the e-i scattering is achieved through the Coulomb potential induced by charged impurities that are three-dimensional-like, the e-i interaction Hamiltonian is given as:

$$H_{e-i} = e^2/(\kappa_i|\mathbf{R} - \mathbf{R}_i|), \quad (31)$$

where $\mathbf{R} = (\mathbf{r}, 0) = (x, y, 0)$ is the coordinate of an electron in ML-TMDs, the impurity is located at $\mathbf{R}_i = (\mathbf{r}_i, z_i) = (x_i, y_i, z_i)$, and κ_i is the static dielectric constant of the medium that contains the impurities. After assuming that the system can be separated into the electrons of interest $|\mathbf{k}; \lambda\rangle$ and the rest of the impurities $|I\rangle$, namely $|\mathbf{k}; \lambda, I\rangle = |\mathbf{k}; \lambda\rangle|I\rangle$, the e-i interaction matrix element is obtained, in the absence of e-e screening, as [27]

$$\begin{aligned} U(\mathbf{q}, \mathbf{R}_i) &= \langle \mathbf{k}'; \lambda', I | H_{e-i} | \mathbf{k}; \lambda, I \rangle \\ &= \frac{2\pi e^2}{\kappa_i q} \sqrt{n_i(z_i)} e^{i\mathbf{q}\cdot\mathbf{r}_i} e^{-q|z_i|} H_{ss'}^{\zeta}(\mathbf{k}, \mathbf{k}') \delta_{\mathbf{k}', \mathbf{k}+\mathbf{q}}, \end{aligned} \quad (32)$$

where $\langle I | I \rangle = [n_i(z_i)]^{1/2}$, with $n_i(z_i)$ being the impurity distribution along the z direction, $\mathbf{q} = (q_x, q_y)$ is the change of the electron wave vector during an e-i scattering event, and $H_{ss'}^{\zeta}(\mathbf{k}, \mathbf{k}') = \langle \mathbf{k}'; \lambda' | \mathbf{k}; \lambda \rangle = A_{s'}^{\zeta}(\mathbf{k}') A_s^{\zeta}(\mathbf{k}) \sum_{j=1}^4 c_{j s'}^{\zeta*}(\mathbf{k}') c_{j s}^{\zeta}(\mathbf{k})$ is the form factor for e-i scattering. Here we have assumed that the impurities are distributed uniformly along the x - y plane. Using Fermi's Golden Rule, the electronic transition rate for scattering

of an electron from a state $|\mathbf{k}; \zeta, s\rangle$ to a state $|\mathbf{k}'; \zeta, s'\rangle$ due to e-i interaction is obtained, in the presence of e-e screening, as [27]

$$\begin{aligned} W_{ss'}^{\zeta}(\mathbf{k}, \mathbf{k}') &= \frac{2\pi}{\hbar} N_i(q) |U_{ss'}^{\zeta}(q)|^2 |H_{ss'}^{\zeta}(\mathbf{k}, \mathbf{k}')|^2 \\ &\quad \times \delta_{\mathbf{k}', \mathbf{k}+\mathbf{q}} \delta[E_s^{\zeta}(\mathbf{k}) - E_{s'}^{\zeta}(\mathbf{k}')], \end{aligned} \quad (33)$$

where

$$U_{ss'}^{\zeta}(q) = \frac{2\pi e^2}{\kappa_i(q + K_{ss'}^{\zeta})},$$

is the screened e-i interaction potential and $N_i(q) = \int dz_i n_i(z_i) e^{-2q|z_i|}$. When a ML-TMDs sheet is placed on a dielectric or magnetic substrate, the background impurities in the ML-TMDs layer and the impurities in the substrate can contribute to the e-i interaction. Normally, the concentrations of these impurities are very hard to determine experimentally. To reduce the fitting parameters for the theoretical study, here we assume that the impurities are effectively located at the interface between the ML-TMDs and the substrate with an effective concentration N_i , i.e., $n_i = N_i \delta(z)$. Thus, $N_i(q) = N_i$ is the areal concentration of the impurities.

Now we consider the case of low temperatures with $T \rightarrow 0$. In such a case, we have $df(x)/dx = -\delta(E_F - x)$ and $f(x) = \Theta(x)$, with $\Theta(x)$ being the unit step-function. The condition of electron number conservation leads to $n_s^{\zeta} = \sum_{\mathbf{k}} f[E_s^{\zeta}(\mathbf{k})]$ so that the Fermi wavevector at the (ζ, s) band is $k_F^{\zeta s} = [4\pi n_s^{\zeta}]^{1/2}$, which is the solution of k from $E_F - E_s^{\zeta}(\mathbf{k}) = 0$. Introducing the electronic transition rate induced by e-i interaction, given by Eq. (33), into Eq. (28), we obtained

$$\begin{aligned} \left[\begin{array}{cc} S_{ss'}^{\zeta x} & T_{ss'}^{\zeta x} \\ T_{ss'}^{\zeta y} & S_{ss'}^{\zeta y} \end{array} \right] &= \frac{N_i n_s^{\zeta}}{2\pi^2 \hbar n_s^{\zeta} A^2} \frac{\text{sign}[G(n_s^{\zeta})]}{G(n_s^{\zeta})} \int_0^{2\pi} d\theta \int_0^{2\pi} d\phi \\ &\quad \times |U_{ss'}^{\zeta}(q)|^2 |H_{ss'}^{\zeta}(\mathbf{k}', \mathbf{k})|^2 [R(\phi, \theta)], \end{aligned} \quad (34)$$

where $\text{sign}(x)$ is the sign function,

$$G(n_s^{\zeta}) = \frac{4E_F^2 - 16\pi A^2 n_s^{\zeta} - \Delta^2 - d_{\zeta}^c d_{\zeta}^v}{4E_F^3 - 2A_2 E_F + A_1}, \quad (35)$$

and

$$[R(\phi, \theta)] = \begin{bmatrix} p_1 \cos \phi & p_1 \sin \phi \\ p_2 \cos \phi & p_2 \sin \phi \end{bmatrix}, \quad (36)$$

where $p_1 = \gamma_{ss'}^{\zeta} \cos(\theta + \phi) - \cos \phi$, $p_2 = \gamma_{ss'}^{\zeta} \sin(\theta + \phi) - \sin \phi$, with $\gamma_{ss'}^{\zeta} = (n_{s'}^{\zeta}/n_s^{\zeta})^{1/2}$. Here, $\mathbf{k}' = (4\pi n_{s'}^{\zeta})^{1/2} [\cos(\theta + \phi), \sin(\theta + \phi)]$, $\mathbf{k} = (4\pi n_s^{\zeta})^{1/2} [\cos \phi, \sin \phi]$, $q = 2\sqrt{\pi} [n_{s'}^{\zeta} + n_s^{\zeta} - 2(n_{s'}^{\zeta} n_s^{\zeta})^{1/2} \cos \theta]^{1/2}$ with θ being the angle between \mathbf{k}' and \mathbf{k} .

III. RESULTS AND DISCUSSIONS

In this study, we take n -type ML-MoS₂ as an example to look into the influence of the proximity effect on

electronic and transport properties of the 2D TMDs system. The material and theoretical parameters for ML-MoS₂ are taken as [1, 30–32]: $A = at = 3.5123$ eVÅ where $a = 3.193$ Å and $t = 1.1$ eV, $\Delta = 1.66$ eV, $\lambda_c = -1.5$ meV, and $\lambda_v = 75$ meV. We note that at present, the experimental and theoretical results of the transport effective electron masses for an electron at the states (ζ, s) , m_s^ζ , are unavailable. Because ML-MoS₂ has a roughly parabolic band structure around the K and K' points [23], here we assume that they are not different far from the average density-of-state effective electron mass, namely we assume $m_s^\zeta \simeq m_e = 0.52m_0$ for ML-MoS₂ [37], with m_0 being the rest electron mass. We consider an air/ML-MoS₂/EuO system where EuO is the magnetic substrate, which can result in the effect of proximity-induced exchange interaction. The dielectric constants for air, a bare ML MoS₂ sheet, and a bare EuO substrate are taken to be, respectively, $\kappa_{air} = 1$, $\kappa_{TMD} = 3.3$ [38] and $\kappa_{Sub} = 23.9$ [39]. Considering the mismatch of the dielectric constants at the ML-MoS₂/EuO interface, we evaluate the effective dielectric constants for ML-MoS₂ and the substrate from the bare dielectric constants using the mirror image method [40]. Thus, we have $\kappa = (\kappa_{air} + \kappa_{TMD})/2 = 2.15$ for ML-MoS₂ and $\kappa_i = (\kappa_{TMD} + \kappa_{Sub})/2 = 13.6$ for the substrate. Because the strength of the Rashba parameter, λ_R , and the effective Zeeman fields for conduction and valence bands, B_c and B_v , can be tuned experimentally, we take them as variable input parameters in numerical calculations. It should be noted that the strengths of B_c and B_v are usually different with different effective Landé g -factors for Bloch states [17]. Because our attention in this study is mainly given to the conduction band, we take $B_v = 5$ meV in all calculations. Since the impurity concentration in a ML-MoS₂/substrate system, n_i , is normally unknown, we take it as a fitting parameter that can be determined by, e.g., using the experimental data of the sample mobility. Furthermore, for a given total electron density in the sample system, n_e , we can determine the Fermi energy E_F by using the condition of electron number conservation,

$$n_e = \sum_{s,\zeta,\mathbf{k}} f[E_s^\zeta(\mathbf{k})]. \quad (37)$$

With the obtained Fermi energy, the electron density at a spin state s in valley ζ in the conduction band can then be calculated via

$$n_s^\zeta = \sum_{\mathbf{k}} f[E_s^\zeta(\mathbf{k})]. \quad (38)$$

A. Electronic band structure and Berry curvature

Some of the basic features of the electronic band structure in ML-MoS₂ have been discussed in our previous research [23]. For convenience of understanding the influence of proximity-induced interactions on electronic

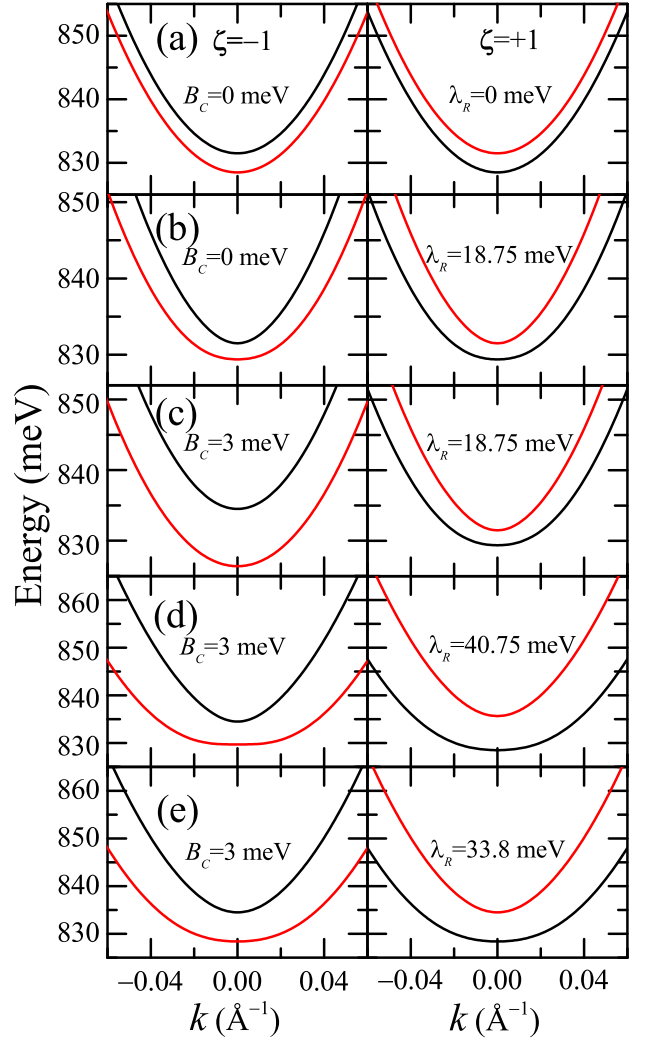


FIG. 1. The electronic band structure of ML-MoS₂ in the presence of proximity induced interactions for conduction subbands in two valleys ($\zeta = \pm 1$). The spin up/down states are represented by red and black curves, respectively. The results with different values of λ_R and B_c as indicated are shown in panels (a)-(e).

and transport properties of ML-MoS₂, to be presented and discussed later, here we present some relevant results about how the Rashba parameter and the strength of EZF would affect the electronic energy levels in the conduction band in ML-MoS₂. In Fig. 1 we show the energy levels in a spin-split ($s = \pm$) conduction band in different valleys ($\zeta = \pm 1$) for different Rashba parameters λ_R and EZF factors B_c . We notice the following features. (i) When $B_c = 0$ the conduction bands in different valleys degenerate (see Figs. 1(a) and (b)). When $\lambda_R = 0$ the splitting of the conduction band is induced by intrinsic SOC λ_c (see Fig. 1(a)). (ii) When $B_c \neq 0$, the degeneracy of the energy levels in different valleys is lifted (see Figs. 1(c) and (d)). (iii) At a fixed B_c , the

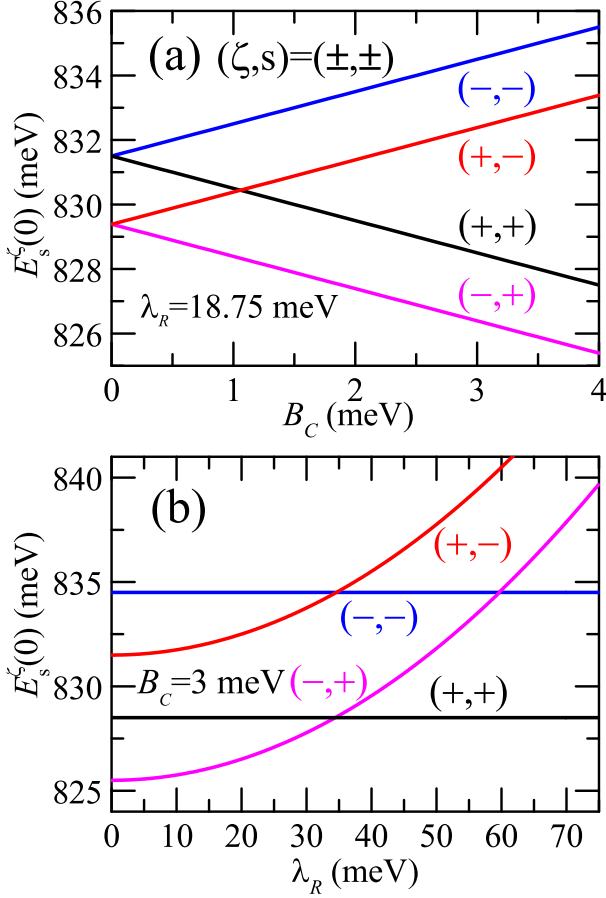


FIG. 2. The energies of the bottoms of four conduction subbands, $E_s^\zeta(0)$ with $k = 0$ and $(\zeta, s) = (\pm, \pm)$, as a function of B_c at a fixed $\lambda_R = 18.75$ meV in (a) and as a function of λ_R at a fixed $B_c = 3$ meV in (b).

energy spacing between two split levels in a certain valley does not increase monotonously with λ_R and a different spin effect can be observed in different valleys (see Figs. 1(c) and (d)). (iv) Interestingly, at a fixed $B_c = 3$ meV, the minimum of the conduction band can be seen in the $\zeta = -1$ valley (see Fig. 1(c)) when $\lambda_R = 18.75$ meV, whereas it can be seen in the $\zeta = +1$ valley (see Fig. 1(d)) when $\lambda_R = 40.75$ meV. And (v) For $\lambda_R = 33.8$ meV in Fig. 1(e), the electronic structure is roughly degenerate for both valleys. These findings indicate that in the presence of proximity-induced interactions, the electronic band structure in ML-MoS₂ depends strongly on λ_R and B_c .

In Fig. 2(a) we plot the bottoms of four conduction subbands, $E_s^\zeta(0)$ with $k = 0$ and $(\zeta, s) = (\pm, \pm)$, as a function of B_c at a fixed Rashba parameter $\lambda_R = 18.75$ meV. We can see that the effective Zeeman field B_c can lead to different energy gaps between spin-split conduction subbands in different valleys. In particular, $E_\pm^\pm(0)$ for four conduction subbands varies linearly with increasing B_c . With increasing B_c , the spin splitting of the conduction band at K' point $\zeta = -1$ always increases,

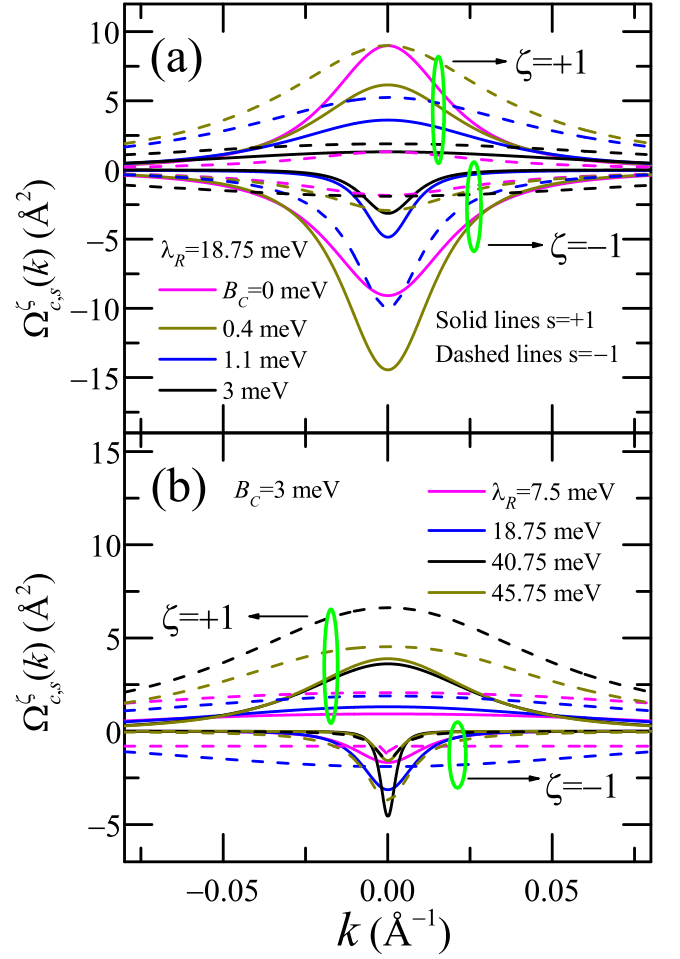


FIG. 3. The Berry curvatures as a function of wavevector k for conduction bands (a) at fixed $\lambda_R = 18.75$ meV with different EZF B_c , and (b) at fixed $B_c = 3$ meV with different Rashba SOC λ_R near K and K' points. The solid and dashed lines refer to the results of spin up and spin down subbands and the green circles are collected for different valleys.

whereas the spin splitting of the conduction subbands at K point $\zeta = +1$ first decreases to zero and then increases. $B_c = 1.1$ meV is a peculiar point at which the energy levels of different spin subbands at the K point are flipped. These results indicate that the effective Zeeman field factor B_c can effectively tune the electronic band structure in the conduction subbands in different valleys; in particular, the energy difference $E_-^+(0) - E_+^+(0)$ can be flipped via varying B_c .

In Fig. 2(b), $E_s^\zeta(0)$ for four conduction subbands are shown as a function of λ_R at a fixed $B_c = 3$ meV. We find that $E_-^-(0)$ and $E_+^+(0)$ in different valleys depend very weakly on λ_R , whereas $E_-^+(0)$ and $E_+^-(0)$ in different valleys increase rather rapidly with λ_R . This implies that the RSOC or λ_R affects mainly the spin-up levels in different valleys. The presence of the proximity-induced exchange interaction (i.e., $B_c \neq 0$) can lift the valley degeneracy and modify the spin splitting. With increas-

ing λ_R , the energy difference between $E_{-}(0) - E_{+}^{-}(0)$ first decreases to zero and then increases, and the energy difference between $E_{-}^{+}(0) - E_{+}^{+}(0)$ always increases. There is also a peculiar point around $\lambda_R = 33.8$ meV at which both $E_{-}^{+}(0) - E_{-}^{-}(0)$ and $E_{-}^{-}(0) - E_{+}^{+}(0)$ approach zero and the lowest conduction subband is changed from $(\zeta, s) = (-, +)$ to $(\zeta, s) = (+, -)$. This effect implies that the lowest conduction subband can be changed from valley K' to valley K via varying the value of λ_R . The results shown in Fig. 2 suggest that the proximity-induced RSOE and Zeeman effect can modulate strongly the spin-split conduction band in different valleys in ML-MoS₂.

As we know, in the presence of an applied electric field \mathbf{E} along ML-MoS₂ film, Berry curvature enters into the semiclassical wavepacket dynamics, and the electrons would gain an anomalous velocity [2, 13] ($v_{sy}^{\zeta} \sim \mathbf{E} \times \Omega_{c,s}^{\zeta}(\mathbf{k})$) perpendicular to the applied electric field. Thus, the Berry curvature would play an important role in affecting the transverse or Hall currents. In Fig. 3, we plot the Berry curvature $\Omega_{c,s}^{\zeta}(\mathbf{k})$ as a function of wavevector \mathbf{k} at valleys K and K' with different EZF and Rashba SOC. As we can see, the EZF B_c and Rashba SOC λ_R can significantly affect the values of Berry curvature. However, the values of Berry curvature in valley K and valley K' are always positive and negative with different EZF and Rashba parameters. This result implies that the directions of the transverse currents contributed by different valleys remain unchanged. The total transverse current is the summation of the contributions from two valleys and the strength of the transverse current could be tuned by varying the EZF and Rashba parameters.

B. Electronic screening length

As shown in Eq. (14), at $T \rightarrow 0$ and $q \rightarrow 0$ limits, the RPA inverse screening length $K_{ss'}^{\zeta}$ is attributed mainly to intra-subband electronic transitions (i.e., $s' = s$). In this study, we only evaluate the electronic screening induced by intra-subband e-e interaction by using Eq. (16). In Fig. 4, we plot the inverse screening lengths $K_{ss'}^{\zeta}$ for four spin-split conduction subbands as a function of electron density n_e at the fixed valence EZF parameter $B_v = 5$ meV and at the low-temperature limit $T \rightarrow 0$ K. Here, different values of B_c and λ_R are used to examine the effect of B_c and λ_R on $K_{ss'}^{\zeta}$. We can see that with increasing electron density, the effect of electronic screening first increases and then depends relatively weakly on n_e , in agreement with the screening effect found in, e.g., graphene [27]. $K_{ss'}^{\zeta}$ differs in spin-split subbands in different valleys. Because $(\zeta, s) = (-, +)$, $(+, +)$ and $(-, +)$ are the lowest electronic subbands (see Fig. 2) for corresponding parameters indicated in Fig. 4, which are always occupied by electrons, K_{++}^{-} in Fig. 4(a), K_{++}^{+} in Fig. 4(b) and K_{++}^{-} in Fig. 4(c) are always non-zero values. The non-zero values of other $K_{ss'}^{\zeta}$ can only be obtained with increasing n_e when the corresponding

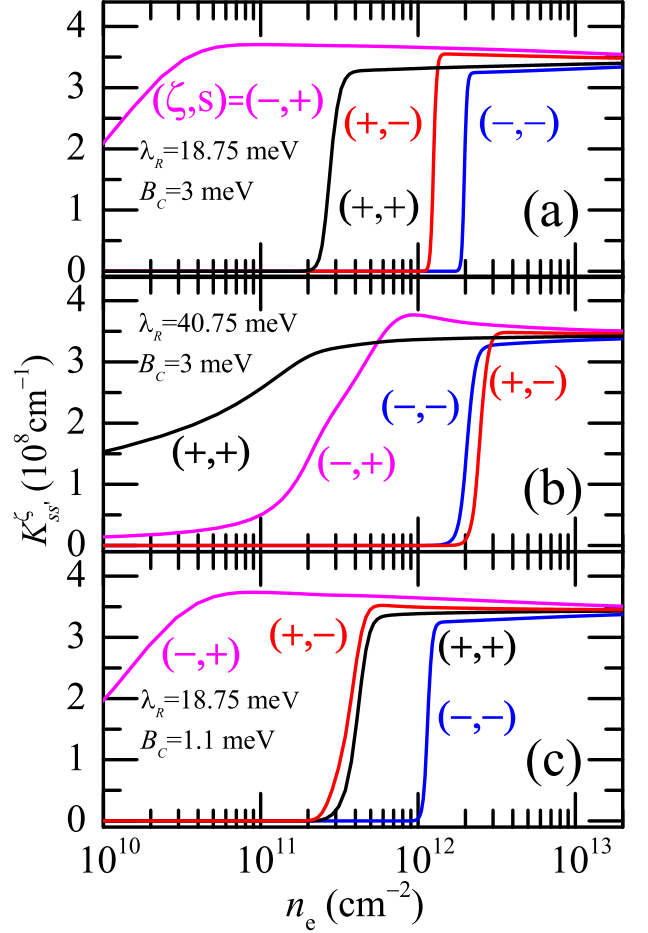


FIG. 4. The inverse screening lengths $K_{ss'}^{\zeta}$ for intra-subband transitions in four spin-split conduction subbands as a function of electron density n_e at $T \rightarrow 0$ for a fixed value of $B_v = 5$ meV. Here, $\lambda_R = 18.75$ meV and $B_c = 3$ meV in (a), $\lambda_R = 40.75$ meV and $B_c = 3$ meV in (b), and $\lambda_R = 18.75$ meV and $B_c = 1.1$ meV in (c).

higher subband becomes populated. At relatively large n_e so that four conduction subbands in both K - and K' -valleys are occupied by electrons, the inverse screening lengths $K_{ss'}^{\zeta}$ for four conduction subbands are approaching roughly the same value with increasing electron density. We note that because the electronic energy spectrum for ML-TMDs is largely parabolic (see Fig. 1), the dependence of $K_{ss'}^{\zeta}$ upon n_e for ML-TMDs is similar to those obtained for semiconductor-based 2D electron gas (2DEG) systems [41]. For ML-MoS₂, the inverse electronic screening length is in the order of 10^8 cm⁻¹, which is in line with the results obtained in semiconductor-based 2DEG systems [41].

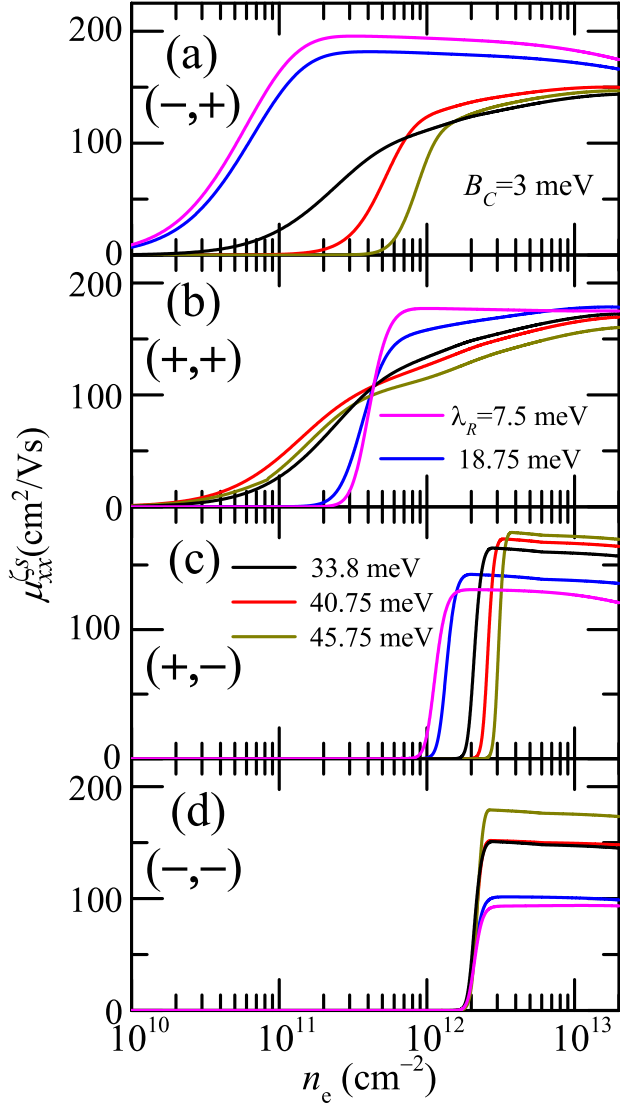


FIG. 5. The longitudinal mobility $\mu_{xx}^{\zeta s}$ in conduction subband $(\zeta, s) = (\pm, \pm)$ in ML-MoS₂ as a function of electron density at a fixed $B_c = 3$ meV for different Rashba parameters λ_R as indicated.

C. Longitudinal and transverse mobilities

In the theoretical approach developed in this study for evaluating the mobilities, the only fitting parameter that we need is the impurity concentration N_i in Eq. (33). Here we take $N_i = 3.98 \times 10^{12} \text{ cm}^{-2}$ for numerical calculations (see the green dot in Fig. 7(a)). This value corresponds to a longitudinal mobility obtained experimentally for an n -type ML-MoS₂ on a SiO₂/Si substrate [42], which is about $174 \text{ cm}^2 \text{ V}^{-1} \text{ s}^{-1}$ at $T = 4$ K and $n_e = 1.35 \times 10^{13} \text{ cm}^{-2}$. The experimental results showed [42] that similar to semiconductor based 2D systems, the longitudinal mobility of ML-MoS₂ depends weakly on temperature when $T < 10$ K. Thus, the results obtained theoretically for $T \rightarrow 0$ from this study can be

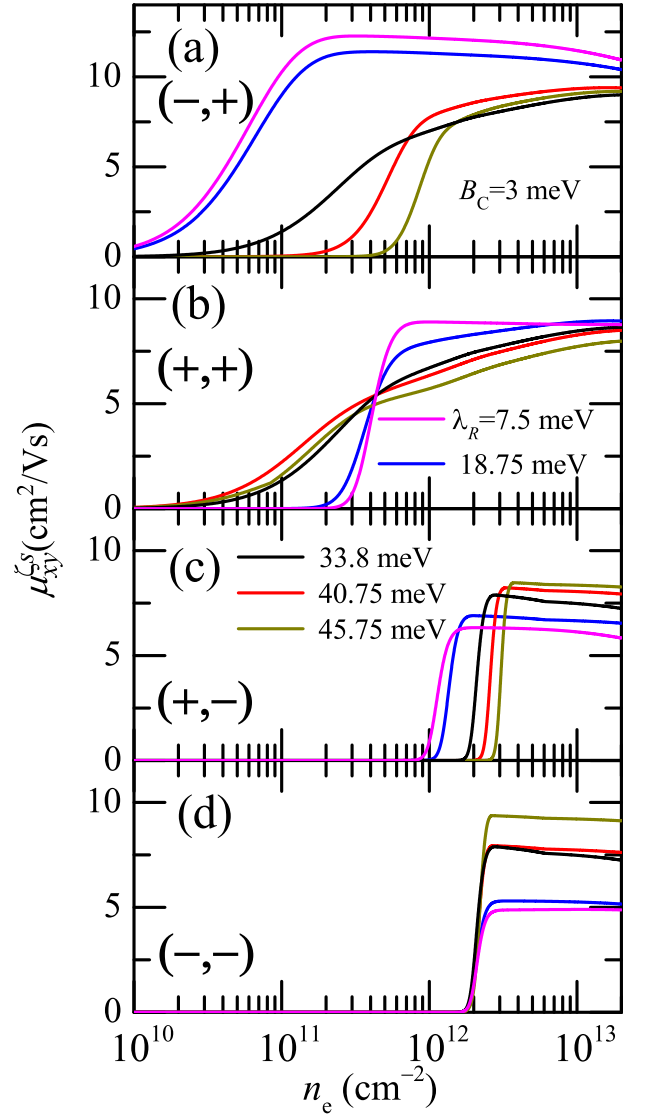


FIG. 6. The transverse or Hall mobility $\mu_{xy}^{\zeta s}$ in conduction subband $(\zeta, s) = (\pm, \pm)$ in ML-MoS₂ as a function of electron density at a fixed $B_c = 3$ meV for different Rashba parameters λ_R as indicated.

applied to reproduce those obtained experimentally at low temperatures $T < 10$ K for ML-MoS₂. Furthermore, we take the transverse mobility in K'/K valley is positive/negative in Eq. (30) due to different directions of the Hall-currents, akin to the application of the magnetic fields along opposite directions.

In the presence of an external magnetic field, the Hall effect can lead to the transverse (Hall) mobility or conductivity [43]. In this study, the transverse mobility comes from the valley Hall effect driven by the pseudo-magnetic field induced by the Berry curvature. Namely the transverse current along the y -direction can be measured in the presence of a driving electric field applied along the x -direction owing to the lift of the valley degeneracy and to the achievement of the spin polarization

in the electronic system [23]. The Berry curvature in ML-TMDs can introduce a pseudo-magnetic field in each spin and valley subband. Thus, the nonzero total transverse (Hall) current or mobility can be observed since the valley Hall effects in two valleys can no longer be canceled out with each other in the presence of proximity-induced interactions. Furthermore, we note that in the presence of proximity-induced interactions, the electron energy is still symmetric along the xy -plane (see Eq. (3)), meaning that it depends only on $|k|$. However, the electron wavefunction is asymmetric in the xy -plane (see Fig. (4)), namely it depends on k_x and k_y . Therefore, the integrations for off-diagonal elements in Eq. (34), which are related to Hall mobility $\mu_{xy}^{\zeta s}$, can be nonzero.

In Fig. 5 and Fig. 6, we show respectively the longitudinal $\mu_{xx}^{\zeta s}$ and transverse or Hall mobility $\mu_{xy}^{\zeta s}$ in conduction subband $(\zeta, s) = (\pm, \pm)$ in ML-MoS₂ as a function of electron density n_e at a fixed EZF $B_c = 3$ meV for different Rashba parameters λ_R . At $B_c = 3$ meV, i) when $\lambda_R < 33.8$ meV, the conduction subbands from the lowest to the highest energies are $(-, +)$, $(+, +)$, $(+, -)$ and $(-, -)$ (see Fig. 2(b)). Thus, μ_{xx}^{-+} and μ_{xy}^{-+} are always nonzero and μ_{xx}^{++} and μ_{xy}^{++} , μ_{xx}^{+-} and μ_{xy}^{+-} and μ_{xx}^{--} and μ_{xy}^{--} can be observed with increasing n_e when they are occupied; ii) when 33.8 meV $< \lambda_R < 59.9$ meV, the conduction subbands from the lowest to the highest energies are $(+, +)$, $(-, +)$, $(-, -)$ and $(+, -)$ (see Fig. 2(b)). Therefore, μ_{xx}^{++} and μ_{xy}^{++} are always nonzero and μ_{xx}^{-+} and μ_{xy}^{-+} , μ_{xx}^{+-} and μ_{xy}^{+-} and μ_{xx}^{--} and μ_{xy}^{--} can be observed with increasing n_e when they become populated; and iii) when $\lambda_R \approx 33.8$ meV, the conduction subbands from the lowest to the highest energies are $(+, +) \approx (-, +)$ and $(-, -) \approx (+, -)$ (see Fig. 2(b)). As a result, μ_{xx}^{++} , μ_{xy}^{++} , μ_{xx}^{-+} and μ_{xy}^{-+} are always nonzero and μ_{xx}^{+-} , μ_{xy}^{+-} , μ_{xx}^{--} and μ_{xy}^{--} can be observed with increasing n_e when they are occupied. When a conduction subband (ζ, s) becomes occupied, both $\mu_{xx}^{\zeta s}$ and $\mu_{xy}^{\zeta s}$ first increase rapidly then depend relatively weakly on n_e with increasing n_e . Moreover, we notice that the longitudinal and transverse mobilities show almost the identical dependence upon the electron density. In the magneto-transport measurements in the presence of an external magnetic field, the longitudinal (drift) and transverse (Hall) mobilities in a 2D electron gas have a relationship [43]: $\mu_{xy} = r_H \mu_{xx} = \sigma R_H$, where r_H is the Hall scattering factor which is a constant for a material or device and R_H is the Hall coefficient. In the present study, the valley Hall effect occurs with the presence of the pseudo-magnetic field induced by the Berry curvature in each spin and valley split subband in a valley nondegenerate ML-TMDs system. Therefore, the contributions to the longitudinal and transverse mobilities from each subband also have the similar features with a proportional relationship. Furthermore, $\mu_{xx}^{\zeta s}$ is about 20 times larger than $\mu_{xy}^{\zeta s}$ when (ζ, s) is well occupied. These results indicate that when $B_c \neq 0$, $\mu_{xx}^{\zeta s}$ and $\mu_{xy}^{\zeta s}$ in an n -type ML-MoS₂ depend strongly on Rashba parameter and electron den-

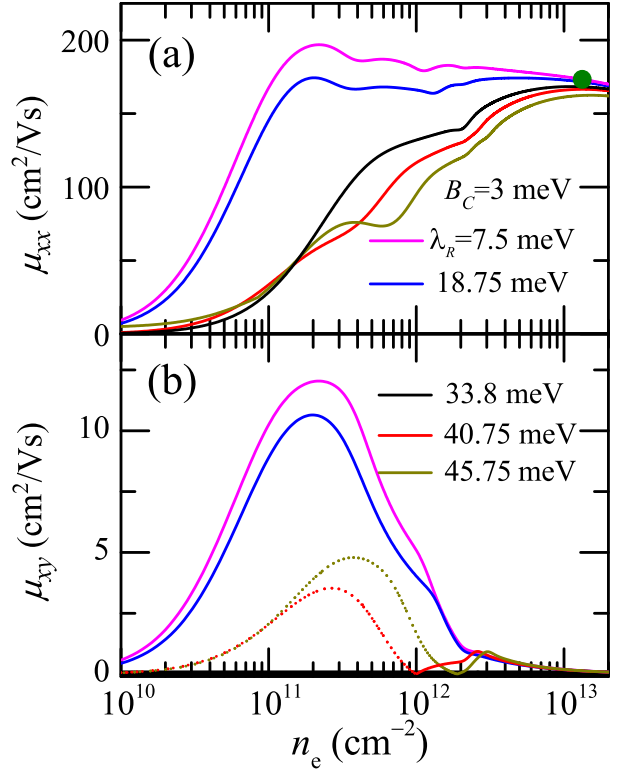


FIG. 7. (a) The longitudinal, μ_{xx} , and (b) the transverse or Hall mobility, μ_{xy} , of ML-MoS₂ as a function of electron density at a fixed EZF $B_c = 3$ meV for different Rashba parameters λ_R as indicated. The green dot at $n_e = 1.35 \times 10^{13} \text{ cm}^{-2}$ in (a) is the mobility obtained experimentally [42], from which we take the value of $N_i = 3.98 \times 10^{12} \text{ cm}^{-2}$ in our calculations. When $\lambda_R \approx 33.8$ meV, $\mu_{xy} \rightarrow 0$ in (b). The dotted part of line corresponds to the reverse direction of the transverse current.

sity.

In Fig. 7, we show the averaged longitudinal μ_{xx} and transverse or Hall mobility μ_{xy} in n -type ML-MoS₂ as a function of electron density n_e at a fixed EZF $B_c = 3$ meV for different Rashba parameters λ_R , obtained by using Eqs. (29)-(30). In low n_e regime μ_{xx} increases with n_e . In high n_e regime, μ_{xx} depends relatively weakly on n_e and μ_{xx} decreases with increasing λ_R . We find that when $B_c \neq 0$, $\mu_{xy} \neq 0$ can be observed and the features of μ_{xy} differ significantly from those of μ_{xx} . (i) μ_{xy} is about 20 times smaller than μ_{xx} ; (ii) μ_{xy} first increases then decreases with increasing n_e . This is due to the fact that at low n_e only the lowest conduction subband is occupied. With increasing n_e and when the higher subbands with different valleys index becomes populated, the valley-currents from different subbands are offset partly and, thus, the overall μ_{xy} decreases with increasing n_e . With further increasing n_e and when all four conduction subbands become occupied, the overall μ_{xy} further decreases and approaches to zero gradually. These results suggest that $\mu_{xy} \neq 0$ can be observed in relatively low n_e in n -type ML-MoS₂. (iii) When $\lambda_R \approx 33.8$ meV, $\mu_{xy} \rightarrow 0$

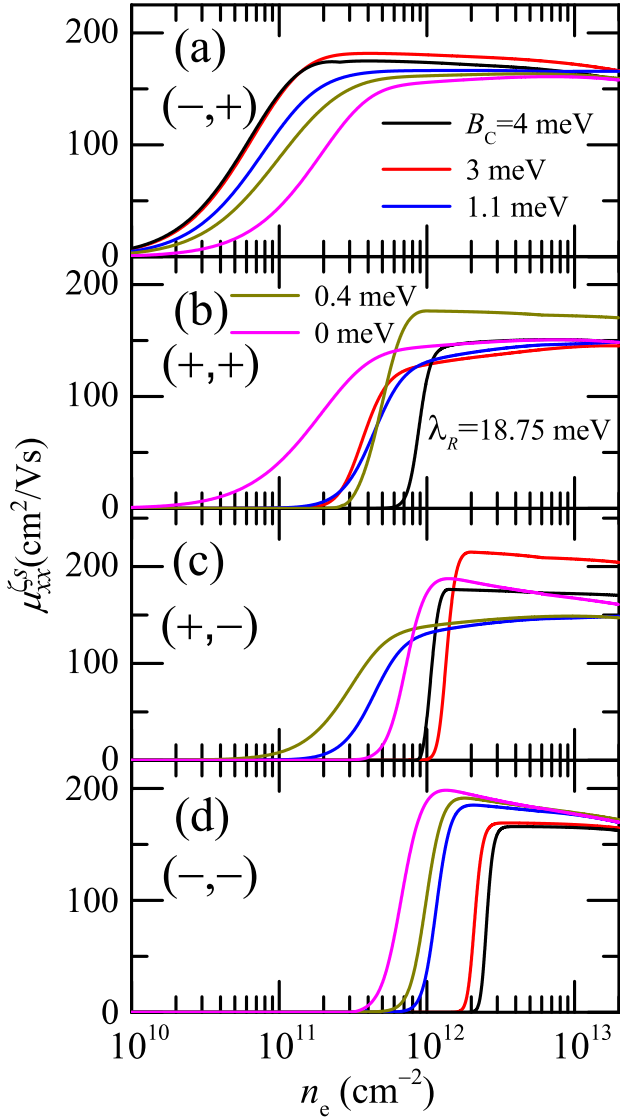


FIG. 8. The longitudinal mobility $\mu_{xx}^{\zeta s}$ in conduction subband $(\zeta, s) = (\pm, \pm)$ in ML-MoS₂ as a function of electron density at a fixed Rashba parameters $\lambda_R = 18.75$ meV for different EFZ B_c as indicated.

because $(-, +) \approx (+, +)$ and $(-, -) \approx (+, -)$ so that $n_+^+ \mu_{xy}^{++} - n_+^- \mu_{xy}^{-+} \rightarrow 0$ and $n_-^- \mu_{xy}^{--} - n_-^+ \mu_{xy}^{+-} \rightarrow 0$; And (iv) interestingly, the sign of μ_{xy} changes at about $\lambda_R = 33.8$ meV and the sign of μ_{xy} would change again after approached to zero with increasing carrier density when $\lambda_R = 40.75$ meV and $\lambda_R = 45.75$ meV [see in Fig. 7(b)], implying that the direction of the Hall current/voltage can be varied through electrically tuning of the Rashba parameter and carrier density through, e.g., the presence of a substrate and/or tuning the applied gate voltage. The transverse mobility has often been investigated in 2D electron gas systems through the Hall effect in magneto-transport measurement [44]. The experimental investigation of the transverse mobility can be conducted in a field effect transistor or encapsulated ML-MoS₂ multi-

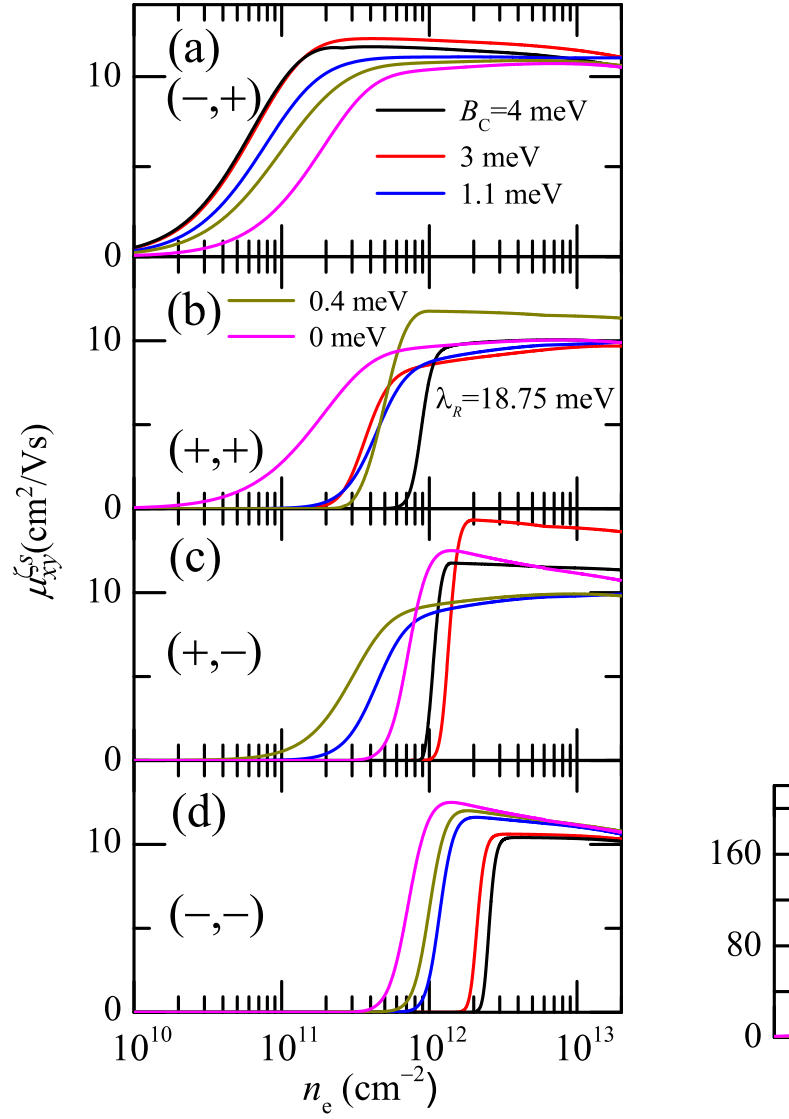


FIG. 9. The transverse or Hall mobility $\mu_{xy}^{\zeta s}$ in conduction subband $(\zeta, s) = (\pm, \pm)$ in ML-MoS₂ as a function of electron density at a fixed Rashba parameters $\lambda_R = 18.75$ meV for different EFZ B_c as indicated.

terminal devices [42, 45].

In Fig. 8 and Fig. 9, we show respectively the longitudinal $\mu_{xx}^{\zeta s}$ and transverse or Hall mobility $\mu_{xy}^{\zeta s}$ in conduction subband $(\zeta, s) = (\pm, \pm)$ in ML-MoS₂ as a function of electron density n_e at a fixed Rashba parameter $\lambda_R = 18.75$ meV for different EFZ B_c . At $\lambda_R = 18.75$ meV (see Fig. 2(a)), i) the lowest conduction subband is always $(-, +)$ so that μ_{xx}^{-+} and μ_{xy}^{-+} are always nonzero; ii) when $B_c < 1.1$ meV, the conduction subbands from the lowest to the highest energies are $(-, +)$, $(+, -)$, $(+, +)$ and $(-, -)$ (see Fig. 2(a)). Thus, μ_{xx}^{-+} and μ_{xy}^{-+} are always nonzero and μ_{xx}^{+-} and μ_{xy}^{+-} , μ_{xx}^{++} and μ_{xy}^{++} and μ_{xx}^{--} and μ_{xy}^{--} can be observed with increasing n_e when they are occupied; ii) when $1.1 \text{ meV} < B_c < 4 \text{ meV}$, the conduction subbands from the lowest to the highest ener-

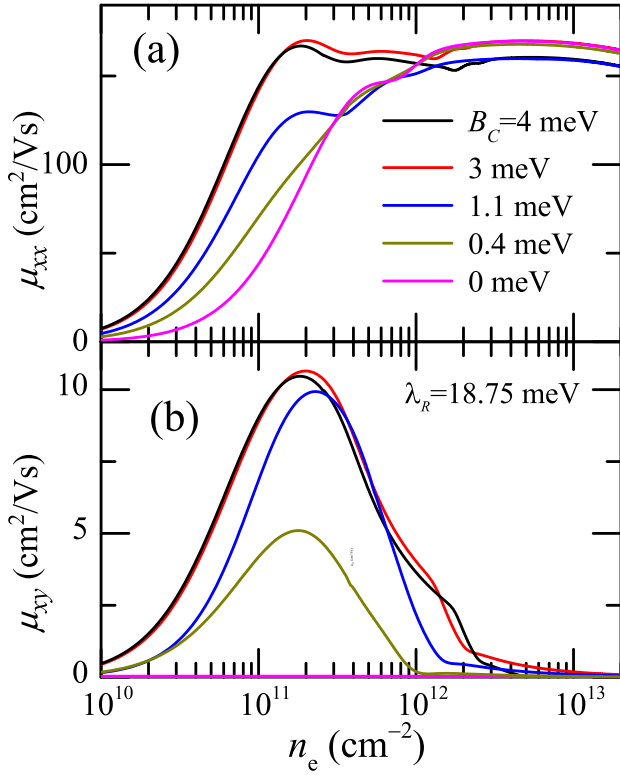


FIG. 10. (a) The transport longitudinal mobility μ_{xx} and (b) the transport transverse or Hall mobility μ_{xy} of ML-MoS₂ as a function of electron density at a fixed Rashba parameter $\lambda_R = 18.75$ meV for with different EZF B_c . In (b), $\mu_{xy} = 0$ when $B_c = 0$.

gies are $(-, +)$, $(+, +)$, $(+, -)$ and $(-, -)$ (see Fig. 2(a)). Therefore, μ_{xx}^{+-} and μ_{xy}^{+-} are always nonzero and μ_{xx}^{++} and μ_{xy}^{++} , μ_{xx}^{+-} and μ_{xy}^{+-} and μ_{xx}^{-+} and μ_{xy}^{-+} can be observed with increasing n_e when they become populated; and iii) when $B_c \approx 1.1$ meV, the conduction subbands from the lowest to the highest energies are $(+, +) \approx (+, -)$ (see Fig. 2(a)). As a result, μ_{xx}^{+-} and μ_{xy}^{+-} are always nonzero and μ_{xx}^{++} , μ_{xy}^{++} , μ_{xx}^{+-} , μ_{xy}^{+-} , μ_{xx}^{-+} and μ_{xy}^{-+} can be observed with increasing n_e when they are occupied. When a conduction subband (ζ, s) becomes occupied, both $\mu_{xx}^{\zeta s}$ and $\mu_{xy}^{\zeta s}$ first increase rapidly then depend relatively weakly on n_e with increasing n_e . Furthermore, $\mu_{xx}^{\zeta s}$ is about 20 times larger than $\mu_{xy}^{\zeta s}$ when (ζ, s) is well occupied. These results indicate that when $\lambda_R \neq 0$, $\mu_{xx}^{\zeta s}$ and $\mu_{xy}^{\zeta s}$ in an n -type ML-MoS₂ depend strongly on EZF parameter and electron density.

In Fig. 10, we show the averaged longitudinal μ_{xx} and transverse or Hall mobility μ_{xy} in n -type ML-MoS₂ as a function of electron density n_e at a fixed Rashba parameter $\lambda_R = 18.75$ meV for different EZF parameters B_c , obtained by using Eqs. (29) and (30). In low n_e regime μ_{xx} increases with n_e . In high n_e regime, μ_{xx} depends relatively weakly on n_e and μ_{xx} decreases with increasing B_c . We find that when $B_c \neq 0$, $\mu_{xy} \neq 0$ can be observed and the features of μ_{xy} differ significantly

from those of μ_{xx} . (i) μ_{xy} is about 20 times smaller than μ_{xx} ; (ii) μ_{xy} first increases then decreases with increasing n_e . This is due to the fact that at low n_e only the lowest conduction subband is occupied. With increasing n_e and when the higher subbands with different valleys index becomes populated, the valley-currents from different subbands are offset partly and, thus, the overall μ_{xy} decreases with increasing n_e . With further increasing n_e and when all four conduction subbands become occupied, the overall μ_{xy} further decreases and approaches to zero gradually. These results suggest that $\mu_{xy} \neq 0$ can be observed in relatively low n_e in n -type ML-MoS₂. (iii) When $B_c \approx 0$ meV, $\mu_{xy} \rightarrow 0$ because the energies of the bands in different valley are degenerate where $(+, -) = (-, +)$ and $(-, -) = (+, +)$ so that $n_-^+ \mu_{xy}^{+-} - n_+^- \mu_{xy}^{-+} \rightarrow 0$ and $n_-^- \mu_{xy}^{--} - n_+^+ \mu_{xy}^{++} \rightarrow 0$. These results indicate that the longitudinal and transverse mobilities can also be tuned by the EZF parameter and carrier density. Comparing Fig. 7 with Fig. 10, we see that both of the Rashba parameter and the EZF parameter B_c can effectively modulated the longitudinal and transverse mobilities. The stronger effect by varying B_c can be observed. However, a large Rashba SOC can reverse the direction of the transverse current with varying electron density. With a relatively large n_e , the effect of the Rashba parameter and the EZF parameter on longitudinal and transverse mobilities becomes weak due to the weakening of the spin polarization in the sample system [23]. When n_e is large enough so that all spin and valley subbands are occupied, μ_{xy} begins to vanish.

In Fig. 11, we plot the averaged longitudinal μ_{xx} and transverse μ_{xy} mobility in n -type ML-MoS₂ as a function of electron density n_e at a fixed Rashba parameter $\lambda_R = 18.75$ meV, and EZF parameters B_c and B_v for different impurity concentrations N_i . As we can see, both μ_{xx} and μ_{xy} decrease with increasing N_i because a larger N_i corresponds to a stronger electron-impurity scattering rate. In our theoretical model developed in this study, the transverse mobility is attributed to both the intrinsic contribution by Berry curvature and the extrinsic contribution by impurity scattering [13, 46]. With a relatively large impurity concentration and at low temperatures, the impurity scattering is the principal channel for electronic scattering rather than phonon scattering. The impurity scattering refers to the skew scattering mechanism, which is proportional to the momentum relaxation time. Since the impurity scattering rate can significantly affect the electron lifetime, the extrinsic impurity scattering would play an important role to affect both the longitudinal and transverse mobilities, as shown in Fig. 11. As far as we know, there is a lack of experimental work for measuring the Hall mobility in ML-TMDs in the absence of an external magnetic field when the valley degeneracy is lifted by proximity-induced interactions, as we predict here. The method of the measurement on such an effect should be the same as that applied for conventional Hall measurement in magneto-transport experiments by using the Hall bar or van der Pauw electrodes.

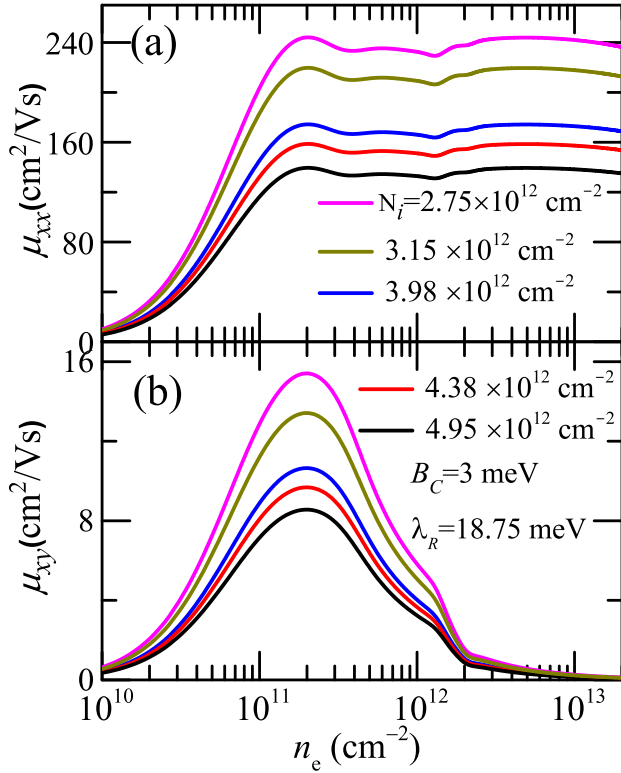


FIG. 11. (a) The transport longitudinal mobility μ_{xx} and (b) the transport transverse or Hall mobility μ_{xy} of ML-MoS₂ as a function of electron density at a fixed Rashba parameter $\lambda_R = 18.75$ meV and EZF parameters $B_c = 3$ meV and $B_v = 5$ meV for different impurity concentrations N_i .

In this study, we considered an n -type ML-MoS₂ laid on a ferromagnetic substrate where the proximity-induced interactions are presented. The electronic screening and transport mobility are contributed by the electrons in the spin-splitting subbands. The electronic structure of an n -type ML-MoS₂/ferromagnetic substrate heterostructure can be effectively tuned by varying the Rashba SOC and EZF via the types of substrate or a perpendicular electrical field. As we know, the carrier density in a 2D system can also be effectively tuned through, e.g., applying a gate voltage. Thus, the electronic screening and transport mobility of a ML-MoS₂ heterostructure system can be tuned by varying these parameters through the state-of-the-art fabrication method of devices and experimental settings. More interestingly, there exists transverse or Hall mobility due to the breaking of valley degeneracy by the EZF. The longitudinal and transverse or Hall mobility can be effectively tuned by the Rashba parameter, EZF, and carrier density. With the unique proximity-induced interactions, a ML-MoS₂-based heterostructure can be a promising material for electronics and valleytronics.

IV. CONCLUSIONS

In this paper, we theoretically investigate the electronic and transport mobility properties of an n -type ML-MoS₂ at low temperature in the presence of proximity-induced interactions such as Rashba SOC and exchange interaction. The electric screening induced by electron-electron interaction is studied under a standard RPA, and the longitudinal and transverse or Hall mobilities are evaluated by using a momentum-balance equation derived from a semi-classical Boltzmann equation where the electron-impurity interaction is considered as the principal scattering event at low temperature. We have examined the roles of Rashba SOC, EZF, and carrier density on affecting the occupation of electrons in spin splitting subbands in different valleys, the inverse screening length, and longitudinal and transverse or Hall mobility of an n -type ML-MoS₂. The main conclusions obtained from this study are summarized as follows.

In a 2D ML-TMDs material such as ML-MoS₂, the Rashba SOC can result in an in-plane electronic spin component. The presence of the proximity-induced exchange interaction can further modify the spin splitting and lift the energy degeneracy for electrons in different valleys. The opposite signs of Berry curvatures in the two valleys would introduce opposite directions of Lorentz force on valley electrons. The inverse screening lengths and transport longitudinal and transverse or Hall mobilities are different in each spin splitting subbands due to the electronic structure and the occupations of electrons in each spin splitting subbands. The total mobility is contributed by each spin splitting subbands. Due to the breaking of valley degeneracy by the EZF, the currents from different valleys are no longer canceled out so that the transverse current or Hall mobility can be observed in the absence of an external magnetic field. The electronic screening, longitudinal mobility, and transverse or Hall mobility can be effectively tuned by the electron density and proximity-induced interactions with the Rashba effect and exchange interaction with an effective Zeeman field. We find that at a fixed effective Zeeman field, the lowest spin-split conduction subband in ML-TMDs can be tuned from one in the K' -valley to one in the K -valley by varying the Rashba parameter. Therefore, we can change the magnitude and direction of the Hall current by varying the Rashba parameter and/or the effective Zeeman field regarding the proximity effect induced by, e.g., the presence of a ferromagnetic substrate and/or applying a gate voltage. As the Hamiltonian for different ML-TMDs is the same but with different material parameters, the behaviors of the longitudinal and transverse (Hall) mobilities should show similar features for different ML-TMD systems in the presence of proximity-induced interactions. The important and interesting theoretical findings in this paper can be beneficial to experimental observation of the valleytronic effect and to gaining an in-depth understanding of the ML-TMDs systems in the presence of proximity-induced interactions. We

hope that the theoretically predictions in this work can be verified experimental in the near future.

ACKNOWLEDGMENTS

This work was supported by the National Natural Science foundation of China (NSFC) (Grants No.

U2230122, No. U2067207, No. 12364009, and No. 12004331), Shenzhen Science and Technology Program (Grant No. KQTD20190929173954826), and by Yunnan Fundamental Research Projects (Grants No. 202301AT070120, and No. 202101AT070166), Y.M.X was supported through the Xingdian Talent Plans for Young Talents of Yunnan Province (Grant No. XDYC-QNRC-2022-0492).

-
- [1] D. Xiao, G. B. Liu, W. Feng, X. Xu, and W. Yao, Coupled Spin and Valley Physics in Monolayers of MoS₂ and Other Group-VI Dichalcogenides, *Phys. Rev. Lett.* **108**, 196802 (2012).
- [2] T. Cao, G. Wang, W. Han, H. Ye, C. Zhu, J. Shi, Q. Niu, P. H. Tan, E. Wang, B. L. Liu, and J. Feng, Valley-selective circular dichroism of monolayer molybdenum disulphide, *Nat. Commun.* **3**, 887 (2012).
- [3] K. F. Mak, D. Xiao, and J. Shan, Light-valley interactions in 2D semiconductors, *Nat. Photonics* **12**, 451 (2018).
- [4] J. R. Schaibley, H. Yu, G. Clark, P. Rivera, J. S. Ross, K. L. Seyler, W. Yao, and X. D. Xu, Valleytronics in 2D materials, *Nat. Rev. Mater.* **1**, 16055 (2016).
- [5] K. F. Mak and J. Shan, Photonics and optoelectronics of 2D semiconductor transition metal dichalcogenides, *Nat. Photonics* **10**, 216 (2016).
- [6] O. Bleu, D. D. Solnyshkov, and G. Malpuech, Quantum valley Hall effect and perfect valley filter based on photonic analogs of transitional metal dichalcogenides, *Phys. Rev. B* **95**, 235431 (2017).
- [7] O. Bleu, D. D. Solnyshkov, and G. Malpuech, Optical valley Hall effect based on transitional metal dichalcogenide cavity polaritons, *Phys. Rev. B* **96**, 165432 (2017).
- [8] H. Dery and Y. Song, Polarization analysis of excitons in monolayer and bilayer transition-metal dichalcogenides, *Phys. Rev. B* **92**, 125431 (2015).
- [9] G. Wang, X. Marie, B. L. Liu, T. Amand, C. Robert, F. Cadiz, P. Renucci, and B. Urbaszek, Control of Exciton Valley Coherence in Transition Metal Dichalcogenide Monolayers *Phys. Rev. Lett.* **117**, 187401 (2016).
- [10] G. B. Liu, W. Y. Shan, Y. Yao, W. Yao, and D. Xiao, Three-band tight-binding model for monolayers of group-VIB transition metal dichalcogenides, *Phys. Rev. B* **88**, 085433 (2013).
- [11] X. Xu, W. Yao, D. Xiao, and T. F. Heinz, Spin and pseudospins in layered transition metal dichalcogenides, *Nat. Phys.* **10**, 343 (2014).
- [12] D. Xiao, W. Yao, and Q. Niu, Valley-Contrasting Physics in Graphene: Magnetic Moment and Topological Transport, *Phys. Rev. Lett.* **99**, 236809 (2007).
- [13] D. Xiao, M. C. Chang, and Q. Niu, Berry phase effects on electronic properties, *Rev. Mod. Phys.* **82**, 1959 (2010).
- [14] Y. D. Lensky, J. C. W. Song, P. Samutpraphoot, and L. S. Levitov, Topological Valley Currents in Gapped Dirac Materials, *Phys. Rev. Lett.* **114**, 256601 (2015).
- [15] Y. K. Kato, R. C. Myers, A. C. Gossard, and D. D. Awschalom, Observation of the Spin Hall Effect in Semiconductors, *Science* **306**, 1910 (2004).
- [16] K. F. Mak, K. L. McGill, J. Park, and P. L. McEuen, The valley Hall effect in MoS₂ transistors, *Science* **344**, 1489 (2014).
- [17] J. Qi, X. Li, Q. Niu, and J. Feng, Giant and tunable valley degeneracy splitting in MoTe₂, *Phys. Rev. B* **92**, 121403(R) (2015).
- [18] C. Zhao, T. Norden, P. Zhang, P. Zhao, Y. C. Cheng, et al, Enhanced valley splitting in monolayer WSe₂ due to magnetic exchange field, *Nat. Nanotechnol.* **12**, 757 (2017).
- [19] B. Yang, M. Lohmann, D. Barroso, I. Liao, et al, Strong electron-hole symmetric Rashba spin-orbit coupling in graphene/monolayer transition metal dichalcogenide heterostructures, *Phys. Rev. B* **96**, 041409(R) (2017).
- [20] A. Soumyanarayanan, N. Reyren, A. Fert, and C. Panagopoulos, Emergent phenomena induced by spin-orbit coupling at surfaces and interfaces, *Nature (London)* **539**, 509 (2016).
- [21] Q. F. Yao, J. Cai, W. Y. Tong, et al, Manipulation of the large Rashba spin splitting in polar two-dimensional transition-metal dichalcogenides, *Phys. Rev. B* **95**, 165401 (2017).
- [22] X. Liang, L. J. Deng, F. Huang, T. T. Tang, et al, The magnetic proximity effect and electrical field tunable valley degeneracy in MoS₂/EuS van der Waals heterojunctions, *Nanoscale* **9**, 9502 (2017).
- [23] X. N. Zhao, W. Xu, Y. M. Xiao, J. Liu, B. Van Duppen, and F. M. Peeters, Terahertz optical Hall effect in monolayer MoS₂ in the presence of proximity-induced interactions, *Phys. Rev. B* **101**, 245412 (2020).
- [24] D. N. Liu and Y. Guo, Strain-tuned spin polarization and optical conductivity in MoS₂/EuS heterostructures, *Phys. Rev. B* **107**, 075430 (2023).
- [25] H. Min, J. E. Hill, N. A. Sinitsyn, et al, Intrinsic and Rashba spin-orbit interactions in graphene sheets, *Phys. Rev. B* **74**, 165310 (2006).
- [26] S. V. Eremeev, I. A. Nechaev, Y. M. Koroteev, P. M. Echenique, and E. V. Chulkov, Ideal Two-Dimensional Electron Systems with a Giant Rashba-Type Spin Splitting in Real Materials: Surfaces of Bismuth Tellurohalides, *Phys. Rev. Lett.* **108**, 246802 (2012).
- [27] H. M. Dong, W. Xu, Z. Zeng, T. C. Lu, and F. M. Peeters, Quantum and transport conductivities in monolayer graphene, *Phys. Rev. B* **77**, 235402 (2008).
- [28] D. Marchenko, A. Varykhalov, M. R. Scholz, et al, Giant Rashba splitting in graphene due to hybridization with gold, *Nat. Commun.* **3**, 1232 (2012).
- [29] P. D. C. King, R. C. Hatch, M. Bianchi, R. Ovsyannikov, et al, Large Tunable Rashba Spin Splitting of a Two-Dimensional Electron Gas in Bi₂Se₃, *Phys. Rev. Lett.* **107**, 096802 (2011).
- [30] H. Z. Lu, W. Yao, D. Xiao, and S. Q. Shen, Intervalley Scattering and Localization Behav-

- iors of Spin-Valley Coupled Dirac Fermions, *Phys. Rev. Lett.* **110**, 016806 (2013).
- [31] Z. Li and J. P. Carbotte, Longitudinal and spin-valley Hall optical conductivity in single layer MoS₂, *Phys. Rev. B* **86**, 205425 (2012).
- [32] Z. Y. Zhu, Y. C. Cheng, and U. Schwingenschlögl, Giant spin-orbit-induced spin splitting in two-dimensional transition-metal dichalcogenide semiconductors, *Phys. Rev. B* **84**, 153402 (2011).
- [33] A. Kormányos, V. Zólyomi, N. D. Drummond, and G. Burkard, Spin-Orbit Coupling, Quantum Dots, and Qubits in Monolayer Transition Metal Dichalcogenides, *Phys. Rev. X* **4**, 011034 (2014).
- [34] A. O. Slobodeniuk and D. M. Basko, Spin-flip processes and radiative decay of dark intravalley excitons in transition metal dichalcogenide monolayers, *2D Mater.* **3**, 035009 (2016).
- [35] H. Ochoa and R. Roldán, Spin-orbit-mediated spin relaxation in monolayer MoS₂, *Phys. Rev. B* **87**, 245421 (2013).
- [36] K. H. Kim and H. W. Lee, Berry curvature in monolayer MoS₂ with broken mirror symmetry, *Phys. Rev. B* **97**, 235423 (2018).
- [37] W. Li, G. Zhang, M. Guo, and Y. W. Zhang, Strain-tunable electronic and transport properties of MoS₂ nanotubes, *Nano Res.* **7**, 518-527 (2014).
- [38] A. Paul and I. Grinberg, Optical Properties of MoS₂, MoSe₂, WS₂, and WSe₂ under External Electric Field, *Phys. Rev. Applied* **17**, 024042 (2022).
- [39] P. Leroux-Hugon, Dielectric Constant of an Exchange-Polarized Electron Gas and the Metal-Semiconductor Transition in Doped EuO, *Phys. Rev. Lett.* **29**, 939 (1972).
- [40] W. Xu, F. M. Peeters, and T. C. Lu, Dependence of resistivity on electron density and temperature in graphene, *Phys. Rev. B* **79**, 073403 (2009).
- [41] W. Xu, Screening length and quantum and transport mobilities of a heterojunction in the presence of the Rashba effect, *Phys. Rev. B* **71**, 245304 (2005).
- [42] B. Radisavljevic and A. Kis, Mobility engineering and a metal-insulator transition in monolayer MoS₂, *Nat. Mater.* **12**, 815-820 (2013).
- [43] T. Ando, A. B. Fowler, and F. Stern, Electronic properties of two-dimensional systems, *Rev. Mod. Phys.* **54**, 437 (2014).
- [44] S. Sucharitakul, N. J. Goble, U. R. Kumar, R. Sankar, Z. A. Bogorad, F.-C. Chou, Y.-T. Chen, and X. P. A. Gao, Intrinsic Electron Mobility Exceeding 10³ cm²/(Vs) in Multilayer InSe FETs, *Nano Lett.* **15**, 3815-3819 (2015).
- [45] X. Cui, G.-H. Lee, Y. D. Kim, G. Arefe, P. Y. Huang, C.-H. Lee, D. A. Chenet, X. Zhang, L. Wang, F. Ye, F. Pizzocchero, B. S. Jessen, K. Watanabe, T. Taniguchi, D. A. Muller, T. Low, P. Kim, and J. Hone, Multi-terminal transport measurements of MoS₂ using a van der Waals heterostructure device platform, *Nat. Nanotechnol.* **10**, 534-540 (2015).
- [46] N. Nagaosa, J. Sinova, S. Onoda, A. H. MacDonald, and N. P. Ong, Anomalous Hall effect, *Rev. Mod. Phys.* **82**, 1539 (2010).